[10] K. J. Eskola, P. Paakkinen, H. Paukkunen, and C. A. Salgado, Eur. Phys. J. C77 , 163 (2017).
[11] E. C. Aschenauer et al. , Phys. Rev. D 96, 114005 (2017).
[12] M. Froissart, Phys. Rev. 123, 1053 (1961).
[13] L. V. Gribov, E. M. Levin, and M. G. Ryskin, Phys. Rept. 100, 1 (1983).
[14] E. Iancu, K. Itakura, and L. McLerran, Nucl. Phys. A708, 327 (2002).
[15] A. H. Mueller and D. N. Triantafyllopoulos, Nucl. Phys. B640, 331 (2002).
[16] D. Kharzeev, E. Levin, and L. McLerran, Nucl. Phys. A748, 627 (2005).
[17] A. Adare et al. [PHENIX Collaboration], Phys. Rev. Lett. 107, 172301 (2011).
[18] L. Zheng, E.C. Aschenauer, J. H. Lee, and B.-W. Xiao, Phys. Rev. D89 , 074037 (2014).
[19] A. Accardi et al., Electron Ion Collider: The Next QCD Frontier, Eur. Phys. J. A52, 2016.

2.2 eRHIC

Christoph Montag and Vadim Ptitsyn
(for the eRHIC study group)
Mail to: montag@bnl.gov
Brookhaven National Laboratory, Upton, NY 11973, USA

2.2.1 Introduction

Brookhaven National Laboratory (BNL) is proposing eRHIC as a cost-effective implementation of the EIC which meets all the requirements on the accelerator formulated in the White Paper. The EIC eRHIC takes advantage of the entire existing Relativistic Heavy Ion Collider (RHIC) facility with only a few modifications, with only modest cost implications. The well-established beam parameters of the present RHIC facility are close to what is required for the highest performance of eRHIC. The addition of an electron storage ring inside the present RHIC tunnel will provide polarized electron beams for collisions with the polarized protons or heavy ions of RHIC.

The eRHIC design must satisfy the requirements of the science program, while having acceptable technical risk, reasonable cost, and a clear path to achieving design performance after a short period of initial operating time. The strategy for arriving at an optimum design that meets these requirements led to an eRHIC design based on an electron storage ring, referred to as Ring-Ring (R-R) design.

The storage ring based design meets or even exceeds the requirements referenced in the Long Range Plan including the upgraded energy reach:

Center-of-mass energy (E_{CM}) of 29 to 140 GeV. The upper limit can only be extended by a significant additional investment in RF equipment; the lower limit is softer and is given by the ability to detect low energy deep inelastic scattered electrons; there is no hard restriction from the accelerator other than reduction in luminosity. The long range plan requires approx. 20 to 100 GeV;

- A luminosity of up to $10^{34}\mathrm{cm}^{-2}\mathrm{sec}^{-1}$; the long range plan requires 10^{33} to $10^{34}\mathrm{cm}^{-2}\mathrm{sec}^{-1}$;

- High polarization of electron and ion beams in arbitrary spin patterns with polarizations well above 50%; the long range plan requires polarizations up to 70%;
- Beam divergences at the interaction point and apertures of the interaction region magnets that are compatible with the acceptance requirements of the colliding beam detector;
- Collisions of electrons with a large range of light to heavy ions (protons to gold ions); the long range plan requires ions as heavy as lead;
- Two interaction regions.

The RHIC tunnel complex incorporates two large experimental halls, with full infrastructure for two major collider detectors. These are at the 6 o'clock position, where the RHIC STAR detector is currently operating, and the 8 o'clock position, home of the RHIC PHENIX detector; see Fig. 1. The design described here allows for eRHIC detectors in each of these areas. In this report we describe in detail the IR configuration for a large general purpose detector in one of these areas (6 o'clock) that could fulfill the requirements for the full range of EIC science questions described above. Our plans for eRHIC include the capability for two such detectors.

The scientific requirements, calling for high luminosity and near-complete angular coverage by the detector, result in an IR lattice that produces a significant degree of chromaticity (energy sensitivity of the beam optics). The non-linear sextupole fields needed to compensate for this effect then limit the dynamic aperture. Calculations motivated by experience at HERA indicate that adding an identical second IR can be achieved without further reduction of the dynamic aperture. We thus plan for detectors at both the IR6 and IR8 positions. In order to avoid unacceptably large beam-beam effects in the case of two experiments, the collider would be operated in a mode where each of the two experiments sees one-half of the bunch crossings; i.e., each experiment receives ½ of the total luminosity.

Highest luminosities can only be achieved by implementing strong cooling of the ion and proton beams to counteract emittance growth by intrabeam scattering (IBS) associated with the corresponding small beam emittances. Cooling of hadron beams with beam energies up to 275 GeV requires novel cooling techniques which are currently being developed and tested in an R&D program at BNL [1].

The design satisfies all requirements and takes into account that beam dynamics limits are not exceeded. In particular, the design parameters remain within the limits for maximum beam-beam tune-shift parameters (hadrons: $\xi_p \leq 0.015$; electrons: $\xi_e \leq 0.1$) and space charge parameter (≤ 0.06), as well as beam intensity limitations. The outline for the eRHIC electron ion collider is shown in Figure 1.

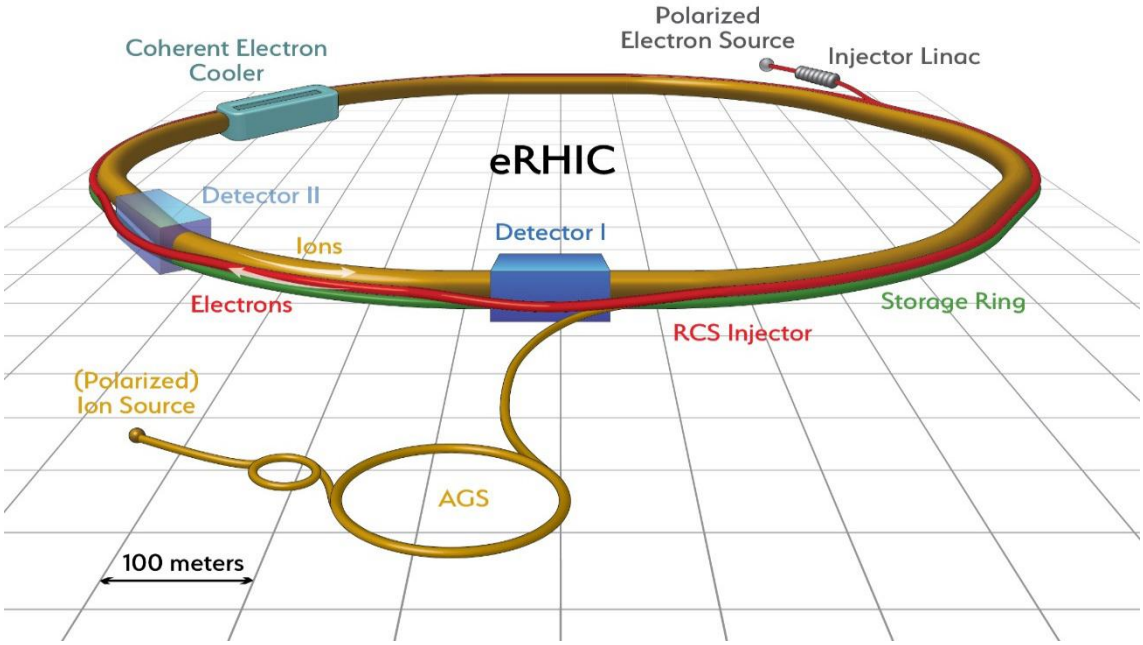

Figure 1: Schematic diagram of the eRHIC layout

Polarized electron bunches carrying a charge of 10 nC are generated in a state-of-the-art polarized electron source. The beam is then accelerated to 400 MeV by a linear accelerator (LINAC). Once per second, an electron bunch is accelerated in a rapid cycling synchrotron (RCS), which is also located in the RHIC tunnel, to a beam energy of up to 18 GeV and is then injected into the electron storage ring, where it is brought into collisions with the hadron beam. The polarization orientation of half of the bunches is anti-parallel to the magnetic guide field. The other half of the bunches have polarization which is parallel to the guide field in the arcs. The Sokolov-Ternov effect [2] will depolarize these electron bunches, in particular at 18 GeV where the (nominal) polarization time constant is smaller, namely 30 min. In order to maintain high spin polarization, each of the bunches with their spins parallel to the main dipole field (of which there are 165 at 18 GeV) is replaced every 6 min. The polarization lifetime is larger at lower beam energies and bunch replacements are less frequent.

The highest luminosity of $10^{34}\mathrm{cm}^{-2}\mathrm{sec}^{-1}$ is achieved with 10 GeV electrons colliding with 275 GeV protons ($E_{\mathrm{CM}} = 105$ GeV). The high luminosity is achieved due to ambitious beam-beam parameters, a flat shape (or large aspect ratio $\frac{\sigma_x}{\sigma_y}$) of the electron and hadron bunches at the collision point, and the large circulating electron and proton currents distributed over as many as 1320 bunches. Table 1 lists the main design parameters for the beam energies with the highest peak luminosity.

Table 1: Maximum Luminosity Parameters

Parameter	***hadron***	***electron***
Center-of-Mass Energy [GeV]	104.9	
Energy [GeV]	275	10
Number of Bunches	1320	
Particles per Bunch [10^{10}]	6.0	15.1
Beam Current [A]	1.0	2.5
Horizontal Emittance [nm]	9.2	20.0
Vertical Emittance [nm]	1.3	1.0
Hor. β-function at IP β_x^* [cm]	90	42
Vert. β-function at IPβ_y^* [cm]	4.0	5.0
Hor./Vert. Fractional Betatron Tunes	0.3/0.31	0.08/0.06
Horizontal Divergence at IP [mrad]	0.101	0.219
Vertical Divergence at IP [mrad]	0.179	0.143
Horizontal Beam-Beam Parameter ξ_x	0.013	0.064
Vertical Beam-Beam Parameter ξ_y	0.007	0.1
IBS Growth Time longitudinal/horizontal [hours]	2.2/2.1	-
Synchrotron Radiation Power [MW]	-	9.18
Bunch Length [cm]	5	1.9
Hourglass and Crab Reduction Factor	0.87	
Luminosity [10^{34}cm-2sec-1]	1.05	

At the lower center-of-mass energies, the beam sizes need to be increased and/or the beam intensities have to be decreased to keep the beam-beam tune shift below the maximum allowed value. At a higher center-of-mass energy, which is achieved by increasing the electron energy to 18 GeV the electron beam intensity has to be reduced to limit the synchrotron radiation power loss to 10 MW. Figure 2 shows the peak luminosity versus center-of-mass energy which will be achieved in eRHIC. In the case of collisions between electrons and ions, the electron-nucleon luminosity is lower, but event rates comparable to the e- p case are achieved.

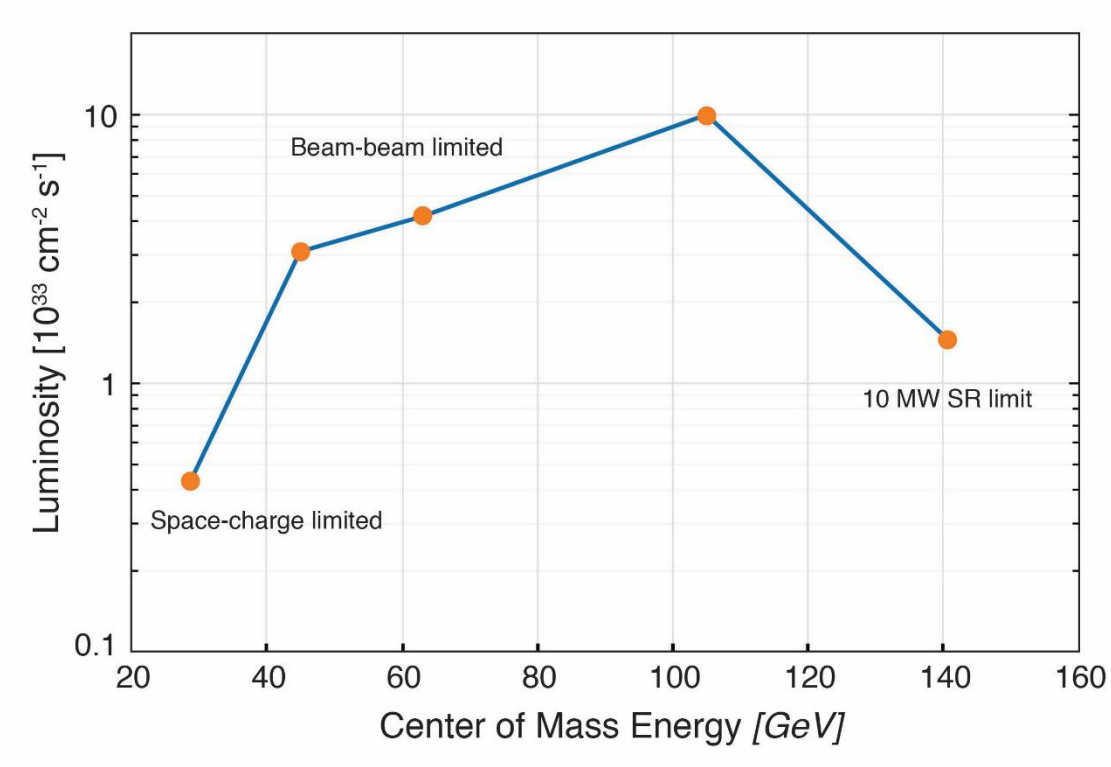

Figure 2: The eRHIC peak luminosity calculation versus center-of-mass energy E_{CM}. The luminosity for low E_{CM} is limited by the beam-beam interaction; at high E_{CM}, the luminosity is limited by the electron beam intensity and the total synchrotron radiation power. A maximum power of 10 MW is chosen to limit the operational costs. This is not a technical limit but a design choice. Solid lines connecting the dots are inserted to guide the eye.

We need to separate the electron and hadron beams quickly after collisions. In order to avoid parasitic crossings without introducing separator magnets and the associated generation of synchrotron radiation, the beams collide under a crossing angle of 22 mrad. Collisions with a crossing angle increase the effective cross section of the beams thereby reducing the luminosity by an order of magnitude. In addition, with a crossing angle, the transverse beam-beam forces depend strongly on the longitudinal position of the particles which generates strong synchro-betatron resonances that affect the beam lifetime and stability. These crossing angle effects are avoided by employing crab crossing using crab cavities. Compensation of the crossing angle by crab cavities is a proven technology that has been demonstrated routinely in the electron-positron collider KEKB, and crab crossing is planned for the high luminosity upgrade of the large hadron collider LHC.

The main elements of eRHIC which have to be added to the existing RHIC complex are:

- A low frequency photocathode gun delivering 10 nC polarized electrons at 1 Hz;
- A 400 MeV normal-conducting S-band injector LINAC;
- A 5 to 18 GeV rapid cycling synchrotron (RCS) in the RHIC tunnel;

- A high intensity, spin-transparent 5 to 18 GeV electron storage ring in the RHIC tunnel with superconducting RF cavities;
- A high luminosity interaction region with 22 mrad crossing angle, crab cavities and spin rotators that allows for a full acceptance detector; a second interaction region is possible and feasible;
- A 150 MeV energy recovery LINAC which provides continuous electron beams for strong hadron cooling;
- A small number of additional buildings which house additional RF power stations and the electron injector.

The eRHIC electron storage ring design is using established and existing technologies from high intensity electron storage rings such as the B-factories of KEK and SLAC, as well as from modern synchrotron light sources.

Other pre-conceptual eRHIC designs, based on the LINAC-Ring (L-R) concept have been presented in the past [3]. As the Ring-Ring design is our chosen solution, the L-R design is presently not further developed and it is not discussed in the body of this report.

2.2.2 **eRHIC Design Concept**

The eRHIC pre-conceptual design provides a path towards a machine with a nominal luminosity of up to $10^{34}\mathrm{cm}^{-2}\mathrm{sec}^{-1}$. The overall concept is to base the design to a large extent on existing technologies, which will greatly reduce the technical risk. This is expected to result in reduced project costs, rapid commissioning, and will provide usable physics data soon after project completion. A design version with somewhat reduced luminosity ("moderate luminosity") is discussed as well in the context of design risk mitigation.

As already mentioned, the eRHIC pre-conceptual design meets the requirements as formulated in the EIC White Paper [4]:

- The design peak luminosity reaches $10^{34}\mathrm{cm}^{-2}\mathrm{sec}^{-1}$ (depending on center-of-mass energy). The electron energy and the luminosity at energies $\mathrm{E}_e \geq 10\ \mathrm{GeV}$ is limited by the power of the synchrotron radiation. A total synchrotron radiation power of 10 MW is considered a reasonable upper limit. This allows a beam energy of 18 GeV together with a luminosity which is still 15% of the maximum luminosity at 10 GeV. For center-of-mass energies of 29 GeV and above the electron energy is at least 5 GeV.

- The center-of-mass energy from 29 to140 GeV is realized by proton energies that range from 41 to 275 GeV, and by electron energies that range from 5 GeV to 18 GeV. RHIC magnets will allow to exceed the present maximum operational energy of 255 GeV since some magnets which presently limit the beam energy will no longer be needed in eRHIC. The lowest eRHIC proton energy is 41 GeV. It is limited by the need to maintain the revolution time for low energy protons. The lowest electron energy is 5 GeV. This is not a hard

limit, but the luminosity will drop below $10^{33}\mathrm{cm}^{-2}\mathrm{sec}^{-1}$ at electron energies below 5 GeV.

- Both electron and hadron beams will be spin polarized with flexible spin patterns. Proton polarization is part of the present RHIC program and can be carried over as-is to eRHIC. The capability of ion polarization (helium and deuterons) will be added by upgrading the Siberian snakes and ion sources, and by improved polarimetry. The electron beam polarization will be enabled by full-energy injection of polarized electron bunches with the desired spin direction (up or down) and frequent electron bunch replacement to ensure a high degree of polarization.

- A transverse momentum detection acceptance for scattered protons from 200 MeV/*c* to 1.3 GeV/c in at least one transverse plane is realized by limiting the divergence angle of the proton beam at the interaction point (IP). Proton β-functions at the IP are chosen such that 50% of all scattered protons with a transverse momentum of 200 MeV/*c* can be detected by forward detectors close to the beam ("Roman Pots"), which limits the achievable luminosity in this configuration. Increasing this lower limit of detectable transverse momentum allows us to decrease the horizontal β-function at the IP substantially, thus increasing the maximum luminosity by a factor of two or more. As the cross section increases steeply with decreasing scattering angle, it is sufficient to operate in this mode for only a small amount of time ($\cong 10\%$), which then has only a correspondingly small impact on integrated luminosity.

The basic assumptions of this design are:

- The electron ring is installed in the existing RHIC tunnel to minimize civil engineering efforts and has the same circumference as RHIC.

- The layout described here admits two interaction regions (IR) and two interaction points (IP). However, the second IR has not yet been integrated into the lattice design and the dynamic aperture assessment is yet to be completed. In case of operation with two collision points, the luminosity is maximized if half of the electron and hadron bunches collide in one of the two interaction points and the other half of the particles collide in the second IP. Luminosities and beam-beam parameters quoted are based on a single beam-beam interaction per turn. In operations with two detectors, each will receive half of the luminosity.

- Electron and hadron beams have identical beam sizes at the interaction point. The beams are flat and the horizontal beam size is larger than the vertical one. At the interaction point, the two beams intersect at a full crossing angle of 22 .in the horizontal plane. The resulting luminosity loss will be largely restored by tilting the bunches around the vertical axis in the IP (perpendicular to the crossing plane) by half the crossing angle using transversely deflecting RF resonators, so-called crab cavities, in the hadron ring. This is mandatory for hadron bunches. Crab cavities in the electron ring

are needed as well to avoid synchro-betatron resonances excited by the collision crossing angle in the electron beam, though their pure geometric effect is negligible.

- Hadron beam parameters are a moderate extrapolation of what has been achieved at RHIC, with the exception that the number of bunches is increased from 110 to up to 1320. The total proton current, however, is increased only by a factor of three. Injection and acceleration will be done with 330 bunches. At the maximum beam energy, in storage mode, the bunches will be adiabatically split in two steps into 1320 bunches. Note that in the absence of strong hadron cooling, a maximum luminosity of $0.4 * 10^{34} cm^{-2} sec^{-1}$ is achievable with 660 bunches.

- A rapid cycling synchrotron (RCS) located inside the RHIC tunnel serves as a polarized full-energy injector for the electron storage ring.

- The maximum electron beam-beam parameter does not exceed $\xi_e = 0.1$, a level that has been routinely achieved at the B-factories KEKB [5][6]. The electron ring will be operated near the integer betatron resonance to mitigate the beam-beam effect while simultaneously minimizing the impact of systematic depolarizing spin resonances.

- The RF power required to replace the power of the synchrotron radiation emitted by the beam is 10 MW. This corresponds to a linear synchrotron radiation power load of 4 kW/m, which is equivalent to $37\ \mathrm{W/mm^2}$ in the arcs. This linear load is less than half of the corresponding value for KEKB [5] and PEP-II [6]. There is no principle hard limit of the RF power but 10 MW is considered a practical upper limit.

2.2.3 **Beam Parameters and Luminosity**

The luminosity of an electron-proton collider is given by:

$$L = H f_b N_p N_e / 4\pi\sigma_x\sigma_y \qquad (1)$$

where N_p and N_e are the number of hadrons and electrons per bunch, respectively, f_b is the bunch frequency, σ_x and σ_y are the RMS beam sizes (assuming they are the same for both beams) given by their beam emittances $\epsilon_{x,y}$ and β-functions at the interaction point (IP) $\beta^*_{x,y}$ as $\sigma_{\{x,y\}} = \sqrt{\epsilon_{x,y}\beta^*_{x,y}}$.
H is a factor reflecting the impact of the hourglass effect (the impact of the variation of the beam cross section along the length of the bunch in collisions) and residual effects of the compensated crossing angle. With the bunch length being close to the vertical beta function at the IP, the factor *H* remains above 0.8.

For eRHIC, the current limits are taken as 1.0 A for the protons and 2.5 A for the electrons, based on the PEP-II [6] operation with 2.1 A at 9 GeV and 3.2 A at 3 GeV.

The numbers of particles per bunch $N_{e,p}$ are constrained by the beam-beam tune shift parameters induced by the bunches upon each other:

$$\xi_{x,y,e,p} = \frac{r_{e,p}}{2\pi}\frac{N_{p,e}}{\gamma_{e,p}\varepsilon_{e,p}}\frac{1}{1+K_{y,x}} \qquad (2)$$

where $r_{e,p}$ are the classical radii of the electrons or protons, respectively, and $K_y = \frac{\sigma_y}{\sigma_x} = \frac{1}{K_x}$.

Combining these two equations and thereby eliminating the emittances yields:

$$L = \frac{1}{e^2\sqrt{r_e r_p}}\frac{1+K_y}{\sqrt{K_y}}(\gamma_e\gamma_p I_e I_p)^{1/2}\left(\frac{\xi_{e,x}\xi_{e,y}\xi_{p,x}\xi_{p,y}}{\beta^*_{e,x}\beta^*_{e,y}\beta^*_{p,x}\beta^*_{p,y}}\right)^{1/4} \qquad (3)$$

In this form, the luminosity is expressed by the limiting factors, the beam currents I_e and I_p, the beam-beam tune-shift parameters $\xi_{x,y,e,p}$, the β-functions at the IP, and the beam size ratio K_y. We see that for flat beams, $K_y \ll 1$, one gets a significant enhancement factor of the luminosity as compared to round beams $(K_y = 1)$. For this reason, the beam parameters are optimized around a value of $K_y = 0.13$ which enhances the luminosity by a factor of $\cong 1.5$ as compared to a round beam scenario.

Colliding beam experience at RHIC suggests the beam-beam parameters ξ_p for the protons are bounded by beam stability considerations at values of $\xi_p \cong 0.015$, while the electrons in a ring-ring collider can, with sufficient synchrotron radiation damping, reach $\xi_e \leq 0.1$ according to experience at the B-factories. Beam currents are assumed to be limited by the values achieved in RHIC (1.2 A) and in KEKB (3.2 A).

High luminosity obviously requires small values of the β-function at the IP. There are a number of constraints which limit the β-function:

- For flat beams, the vertical β-function at the IP is smaller than the horizontal one. The vertical β-function is limited by the length of the proton bunch via the hourglass effect. The proton bunch length in turn is limited by intra-beam scattering. The minimum value is about 5 cm for the highest luminosity case with 1320 bunches.

- An important part of the EIC physics program is the measurement of the spatial distribution of the gluon density of the hadrons. This requires detection of protons which are scattered under a small angle. The acceptance for such low transverse momentum scattered protons (low-p_t) depends strongly on the

horizontal divergence of the beam at the IP and gives rise to another limitation for the horizontal β-function and K_y. The horizontal divergence is proportional to $\frac{1}{\left(\beta^*_{xp}\right)^{1/2}}$. In order to accept scattered particles with $p_t = 200\ \mathrm{MeV}/c$, the horizontal β-function of the hadron beam should be about 1 m. The design values of are$\beta^*_{xp} = 90$ cm and $\beta^*_{yp} = 5$ cm.

- Small β-functions at the IP imply large β-functions in the strong final focus quadrupoles. Very large β-functions in quadrupoles cause a strong effect on the tune and the optics for off-energy particles, referred to as chromaticity. Chromaticity needs to be compensated to provide sufficient space for a stable working point for the beam in-between nonlinear resonances. Chromaticity correction is accomplished by nonlinear sextupole fields in the accelerator arcs. This in turn introduces a dynamic aperture limit and increases the width of nonlinear resonances to be avoided by reducing the tune footprint. Sufficient beam lifetime requires a minimum dynamic aperture which equals 10 times the transverse RMS beam size. Beyond a certain value of chromaticity the stability requirements for the beam cannot be fulfilled. This threshold value depends on other parameters such as phase advance per arc FODO cell and number of sextupole families. An approximate rule is that the IR chromaticity should not contribute more than about one third to the total natural chromaticity.

In summary, the general concept of achieving high luminosity is the same as that for e^+e^--colliders:

Luminosity is increased by running with the highest beam currents, using flat beams, low emittances, and low β functions at the IP. Focusing magnets are installed as close as possible to the IP. The beam current is distributed over many, shortly spaced bunches, while the charge per bunch is relatively low. These choices mandate a crossing angle collision geometry.

Table 1 shows the beam parameters for the highest luminosity. Highest luminosity is achieved for an electron beam energy of 10 GeV and for a hadron energy of 275 GeV. Both the β^* and emittances, of both protons and electrons, are larger in the horizontal than in the vertical plane, resulting in flat beam profiles at the IP. Unequal emittances are natural for the electrons in a storage ring. For protons, however, the beam first needs to be pre-cooled at low energies, using electron cooling. Subsequently, kicker noise is applied in the horizontal plane to increase the horizontal emittance to its desired value. Experimentally, it is known that such emittance asymmetries will be stable in RHIC for long storage times.

Maximum luminosity is achieved with an electron beam energy of 10 GeV and a proton energy of 275 GeV which corresponds to a center-of-mass energy of 105 GeV. For larger electron energies, the rapidly increasing synchrotron radiation power scales with the electron energy to the 4^{th} power, $P \sim E_e^4$. This requires reducing the electron current by the same factor to keep the total synchrotron radiation power below the design limit of 10 MW. At the highest energy, the electron current is only 0.26 A, nine times smaller than the maximum value. The loss in luminosity is mitigated by

decreasing the number of bunches by a factor of four and adjusting the transverse beam parameters. The increase of electron beam emittance, which scales as E_e^2, is compensated by increasing the phase advance in the arcs from 60 degrees per FODO cell to 90 degrees per FODO cell. The overall result is that the luminosity is reduced by a factor of seven as compared to the maximum value achieved at 10 GeV.

These considerations result in the luminosity versus center-of-mass energy as shown in Figure 2.

The parameters shown in Table 1 are derived with the assumption that the proton beam emittance will remain at the very small values of $\varepsilon_x = 9.3$ nm and $\varepsilon_y = 1.3$ nm. However, the dense hadron beam is subject to substantial emittance growth due to intrabeam scattering (IBS). IBS must be counterbalanced by strong cooling of the hadron beam to maintain emittance and bunch length over a reasonable amount of time. This time needs to be much larger than the time it takes to replace a depleted hadron beam. Several schemes for strong cooling are considered that promise to yield sufficiently fast cooling rates to balance emittance growth at the operational parameters of eRHIC. One of these schemes called "Coherent Electron Cooling" [7] is being tested experimentally.

As already mentioned the design must enable detection of scattered protons with a minimum transverse momentum of $p_t = 200\ \mathrm{MeV}/c$, which at a hadron beam energy of 275 GeV corresponds to a scattering angle of $730\ \mu\mathrm{rad}$. The RMS divergence of the proton beam at the IP must not exceed one tenth of this minimum scattering angle, $\sigma' \leq 73\ \mu\mathrm{rad}$. This requirement, however, may be violated in the vertical plane, provided the beam divergence in the horizontal plane meets the requirement. A horizontal RMS beam divergence of $56\ \mu\mathrm{rad}$ allows detection of 50% of all scattered protons with a transverse momentum of 200 MeV/*c*. In order to improve low p_t acceptance eRHIC may be operated for a short time, say 10% of the time, with larger β^* and lower divergence and thus full acceptance. Because of the large cross section for small p_t, in a short amount of time a large amount of data can be collected so that there is eventually an equal amount of data at all p_t values. This scenario substantially increases the effective luminosity of the facility.

So far we have only discussed electron-proton collisions. Most of the considerations discussed in this section apply to ions with only a few exceptions that are addressed below.

Ions are characterized by the number of nucleons, *A*, and the electrical charge *Ze,* with $A \cong 2Z$. The beam-beam tune shift of the electrons, assumed to be at the maximum tolerable value for the collision parameters with protons, is proportional to *Z,* which for protons is equal to one. In order to maintain the electron tune shift value in collisions with ions, the number of ions per bunch, N_i has to be reduced by a factor *Z*. The beam-beam tune shift for the hadrons is also proportional to *Z* but is inversely proportional to *A*. Thus the ion beam-beam tune shift is reduced approximately by a factor of two for a constant number of electrons. In principle, we could benefit from the reduced tune shift and increase the number of particles in the electron bunch by a factor of two. However, this would increase the electron beam current by a factor of two, which is not possible. In conclusion, the electron-ion luminosity is reduced by a factor of *Z*. However, most of

the cross sections in electron-ion collisions will increase by a factor of A compared to e-p cross sections. Therefore, the event rate of electron-ion collisions is expected to increase by a factor of approximately two in electron-ion collisions as compared to electron-proton collisions in eRHIC.

2.2.4 **Moderate Luminosity without Strong Hadron Cooling**

The highest luminosity of the electron-ion collider depends on the feasibility of strong hadron cooling. The eRHIC approach to strong hadron cooling is coherent electron cooling. This is a novel approach which has never been tested experimentally. However, a proof-of-principle experiment is underway which aims to demonstrate this technique using a free electron laser (FEL) as an amplification mechanism. This experiment is scheduled to produce results by the end of FY18. Nevertheless, the feasibility of this approach cannot be guaranteed at this point, which constitutes a high technical risk for achieving the highest luminosity goal of eRHIC. In the following, we discuss how this risk is mitigated.

There are three ways this mitigation could be achieved:

- Coherent electron cooling with R_{56} enabled micro-bunching as an alternative coherent electron cooling amplification mechanism;
- Magnetized bunched beam electron cooling as an alternative hadron cooling scheme;
- An eRHIC design solution with a somewhat reduced peak luminosity.

The micro-bunching based coherent electron cooling might suffer from the same principle uncertainties as the FEL based scheme. It is nevertheless an attractive option that promises to need less current for the cooling electron beam. While we are pursuing this very promising approach, we do not consider it to be the primary way to mitigate the CeC performance risk.

Magnetized bunched beam electron cooling is a novel technique as well that has not yet been demonstrated. However, non-magnetized bunched beam cooling is being implemented for the RHIC low energy run in FY19 and FY20. There is no known reason why the fact that the beam is bunched would affect the otherwise well proven electron cooling mechanism. However, magnetized bunched beam cooling for 275 GeV hadron beams requires a complicated, expensive, and very challenging setup which, even though it might technically work, is considered prohibitive from a cost point of view. Independent of cost, the required beam current of the electron cooler is in the order of 1 A. This exceeds by far the present capability of CW high brightness electron sources. Furthermore, such currents require an energy recovery LINAC (ERL). However, the virtual beam power in the ERL would extend into the 100 MW regime, a factor 100 above state-of-the-art.

Our preferred solution is to consider a scheme with a more moderate but still more than sufficient peak luminosity which does not require strong hadron cooling as a realistic and credible way to mitigate the risk associated with a very high luminosity solution. The parameters of this solution will be discussed in this section.

The main difference between the high and moderate luminosity version is reducing the number of bunches by a factor of two, from 1320 to 660 bunches, which is still 6 times larger than the number of bunches in present RHIC. IBS is reduced by an increase of the vertical emittance of the protons by a factor 6.5 compared to the version with strong hadron cooling. Re-optimization of the beam optical parameters at the collision point and lengthening the proton bunches from 5 cm to 7 cm leads to the parameters as shown in Table 2. These hadron beam parameters imply IBS emittance growth times of more than nine hours in both the horizontal and the longitudinal plane which eliminates the need for strong hadron cooling.

The electron bunch current is more critical for this solution. The product of average current and bunch current, which is the figure-of-merit for heating of the vacuum system, increases by a factor of 1.5 but remains still within the margins given by the cooling of the RF shielded bellows, the temperature limit of the RF buttons, and other sensitive vacuum equipment. The resulting luminosity is still $4.4 * 10^{33}\mathrm{cm}^{-2}\mathrm{sec}^{-1}$. The full set of parameters is shown in Table 2.

Table 2: Moderate Luminosity Parameters for 10 GeV electrons on 275 GeV hadrons.

Parameter	***hadron***	***electron***
Center-of-Mass Energy [GeV]	104.9	
Energy [GeV]	275	10
Number of Bunches	660	
Particles per bunch [10^{11}]	1.05	3.0
Beam Current [A]	0.87	2.48
Horizontal Emittance [nm]	13.9	20
Vertical Emittance [nm]	8.5	4.9
Horizontal β_x^* at IP [cm]	90	63
Vertical β_y^* at IP [cm]	5.9	10.4
Horizontal Divergence at IP [mrad]	0.124	0.179
Vertical Divergence at IP [mrad]	0.380	0.216
Horizontal Beam-Beam Parameter ξ_x	0.015	0.1
Vertical Beam-Beam Parameter ξ_y	0.005	0.083
IBS Growth Time long/hor [hours]	10.1/9.2	-
Synchrotron Radiation Power [MW]	-	9.1
Bunch Length [cm]	7	1.9
Luminosity [10^{33}cm^{-2}sec^{-1}]	4.4	

The luminosities for different center-of-mass energies are obtained using the same considerations as the ones outlined for the high luminosity solution. The electron beam

current for energies larger than 10 GeV is reduced to limit the total energy loss of the beam to 10 MW. At lower energies, the parameters are optimized for the reduced beam-beam tune shift limits for the electrons. Figure 3 shows how the luminosity varies with center-of-mass energy.

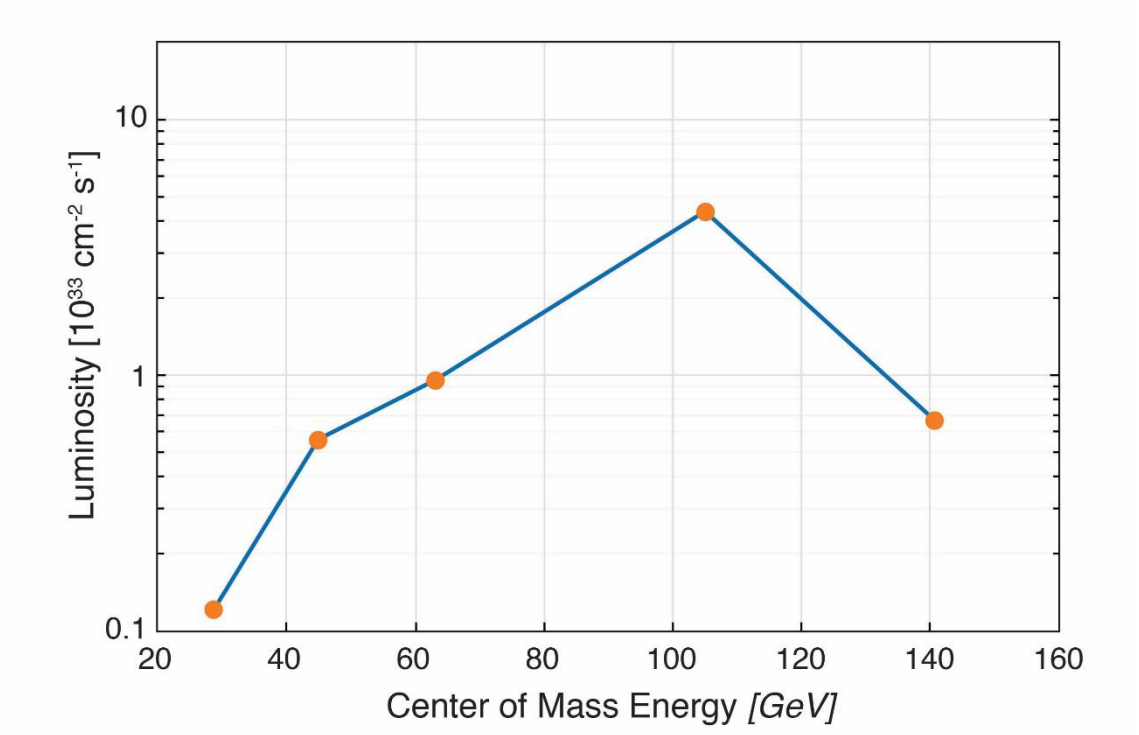

Figure 3: Moderate eRHIC peak luminosity versus center-of-mass (CM) energy. The luminosity for low CM energy is limited by the beam-beam interaction; at high CM energy, the luminosity is limited by the electron beam intensity and the total synchrotron radiation power, the limit of which has been set to 10 MW for cost reasons.

The luminosity without strong cooling is within a factor of 3 of the high luminosity goal of eRHIC. This luminosity satisfies the requirements on the performance of an EIC formulated in the Nuclear Physics White Paper and thus this more moderate eRHIC performance still provides access to the entire EIC physics program. The moderate luminosity solution has been reviewed and characterized as realistic and implementable without major technical risk. We conclude that this performance would, at least initially, fully satisfy the needs of the physics program. This would provide more time to develop, implement and optimize strong hadron cooling, thereby greatly reducing the technical risk associated with strong hadron cooling. In addition, this solution would lead to a substantial initial cost saving.

In summary, we conclude that the solution with moderate luminosity not only mitigates the risk of strong hadron cooling falling short of expectations but offers in addition initial substantial construction cost savings.

2.2.5 **Beam-Beam Dynamics**

The eRHIC approach to achieving stable beam-beam interactions is similar to the HERA approach:

Each beam is assumed to achieve the same beam-beam tune shift values as they did when colliding with a beam of the same species. The beam-beam tune shift is an established measure of characterizing the strength of the highly nonlinear interaction of the two beams.

However, for eRHIC, this approach is applied on a much higher level of beam-beam strength than HERA. For this reason, comprehensive simulation studies have been performed to ensure that the beams remain stable in collisions and that the hadron beam does not suffer from strong emittance growth when colliding with the electron beam. Long-term slow emittance growth is investigated by so-called weak-strong beam-beam simulations. With this method one beam is considered static in its transverse and longitudinal dimensions. This is the equivalent of treating it as a static external field. The other beam is described by single particles which are launched in phase space and whose trajectories are tracked in a complete dynamic model over a large number of turns. This study did not reveal any strong hadron beam emittance growth for the operational parameters of eRHIC.

The other effect which might compromise the performance of an electron-ion collider is a strong coherent interaction between the two beams. Such interactions have been observed occasionally in HERA, but could not be studied systematically. If such a coherent beam-beam instability occurs, the hadron beam transverse phase space will filament quickly, which corresponds to a strong effective emittance growth. This renders the hadron beam completely useless for high luminosity collision operations.

This issue was investigated for eRHIC parameters using so-called strong-strong beam-beam simulations. Both beams are described by super-particles in a complete dynamical model. The particle distributions at the collision point are used to generate a realistic beam-beam force. Much mathematical finesse is required to suppress artificial noise due to the fact that the number of super-particles is much smaller than the number of particles in a real beam. These methods are not well suited to investigate long term stability of the beam but are designed to describe short term strong dynamic effects.

The simulations for eRHIC performed with the computer codes BBSS [8] and BeamBeam3D [9] indeed revealed a coherent instability such as observed in HERA. A clear instability threshold has been found for beam-beam tune shift values of the hadron beam which are twice as large as the eRHIC design parameters. Figure 4 shows the result of this simulation.

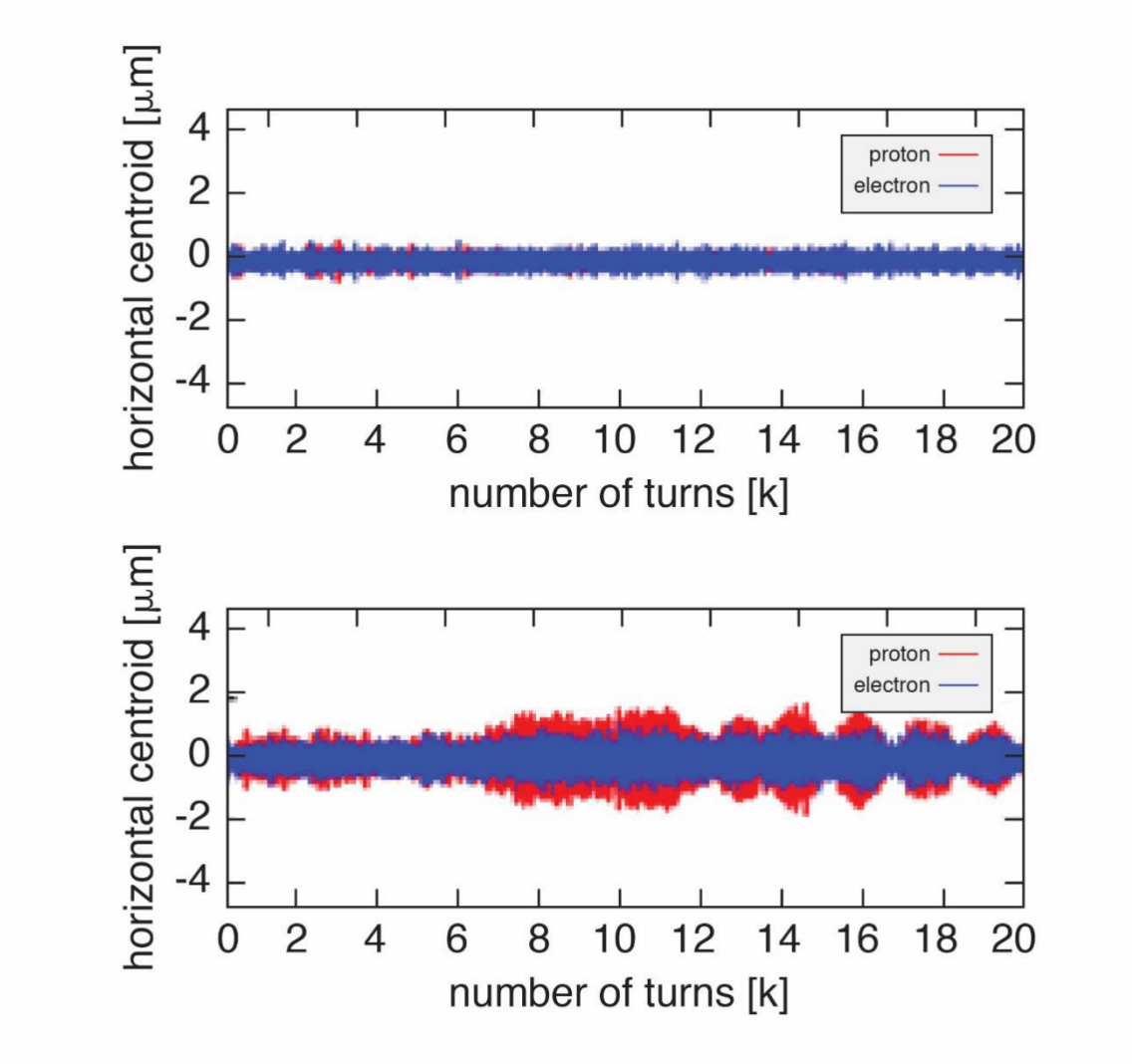

Figure 4: Coherent beam-beam instability as seen by strong-strong beam-beam simulations using the code BBSS. The number of protons in the upper plot is at 1.6 times the eRHIC design value of 10^{11}. In the lower plot, the number of protons is increased to twice the design value. In this case both beams perform unstable betatron oscillations. Such oscillations will blow up the hadron beam emittance

The conclusion of the beam-beam dynamics study is that while the eRHIC beam-beam parameters are fairly aggressive, the simulations predict stable beams in collisions with only small long-term emittance growth. Further studies are still in progress at this stage of the eRHIC design. Additional detrimental effects could still arise due to the imperfect compensation of the crossing angle and residual dynamic effects such as synchro-betatron resonances as well as due to imperfection and spurious dispersion in the crab cavities.

2.2.6 **Layout of the Interaction Region**

The layout of the interaction region (IR) fulfills the following requirements:

- To achieve small beam cross sections and high luminosity, the beams are strongly focused at the interaction point (small β^*) by low-β quadrupole magnets, also referred to as final focus quadrupoles.
- The final focus quadrupoles must have sufficient aperture for the large beam size at their location.

- Large contributions to the chromaticity, which is a set of parameters characterizing the energy sensitivity of the beam optics, are generated in the low-β quadrupoles. Chromaticity needs to be compensated by sextupole fields which, in turn, limit the dynamic aperture. The IR design balances small β^* and tolerable values of chromaticity.

- The colliding beam detector requires a large acceptance of protons scattered off the collision point. Therefore, we do not place accelerator components inside the detector within 4.5 m from the IP. The low-β quadrupoles have a large aperture so that scattered protons and neutrons can be detected by detector elements placed further downstream.

- The beam divergence and therefore the minimum β^* is restricted to enable detection of forward scattered protons with transverse momenta as small as $p_t = 200\ \mathrm{MeV}/c$ These particles are then outside the 10σ proton beam envelope and are detectable by near-beam detectors, so-called "Roman Pots", which are placed on the forward hadron beam pipe.

- The beams collide under a crossing angle of 22 mrad to separate the electron and proton beams quickly, to avoid parasitic collisions, and to provide space for a neutron detector in the forward direction and the luminosity detector in the forward electron direction. An important factor is the large bunch frequency of up to 112 MHz, which corresponds to only 9 nsec bunch spacing, required for high luminosity. The crossing angle effects, in particular enlarged transverse beam size and excitation of synchro-betatron resonances, must be compensated for by using so-called crab cavities, transverse RF resonators which kick the head and the tail of the proton and electron bunches in opposite directions in the plane of the crossing angle. These cavities are placed at a horizontal betatron phase advance of $\pi/2$ from the interaction point (IP) on both the rear and the forward side, forming a 180 degree bump. This causes the bunches to be tilted in the horizontal plane by exactly half the crossing angle at the IP, and provides (ideally) the same collision geometry as head-on collisions, thereby avoiding synchro-betatron coupling.

- Strong synchrotron radiation which might be generated by the electron beam can destroy sensitive detector equipment and make data-taking impossible. Therefore, we argue that the electron beam must not experience dipole fields in the interaction region (IR), certainly not on the forward side upstream of the IP. This is another strong reason why the two beams must collide at a crossing angle. Synchrotron radiation generated in the low-β quadrupoles on the rear-electron side should be absorbed on the rear side of the IR as far as possible from the detector in order to minimize backscattered photons. This requires an extra large

aperture for the electron low-β quadrupole magnets on the downstream side of the IP.

- Both the hadron and electron beams are spin polarized. Polarization is only stable if the polarization direction coincides with the direction of the guide field in the arcs. In collisions, the polarization is oriented longitudinally. Thus the IR design accommodates pairs of spin rotators which accomplish longitudinal spin at the IP and vertical spin in the arcs. The spin rotators in the hadron ring already exist and are unchanged in this design.
  The electron beam spin rotators are based on a sequence of strong solenoids and horizontally bending dipoles interleaved with quadrupoles which are tuned for canceling the *x*-*y* coupling introduced by the solenoids. While the dipole bending angle is fixed, a proper setting of the solenoids allows the correct spin rotation at all energies between 5 and 18 GeV.
  One of such rotators is required on each side of the IP. The beam transport between the rotators is "spin transparent". This means that the magnetic fields in quadrupole magnets experienced by a particle performing betatron and synchrotron oscillations cancel between the spin rotators. This translates into beam optics spin matching conditions.

- The IR layout must provide room for a luminosity monitor on the rear side. This monitor detects hard γ-rays that are generated in the Bethe-Heitler process and exploited for luminosity measurement. The dipole magnet bending the electrons away from the path of the γ beam is at the same time a spectrometer magnet for the off-momentum electrons generated by the Bethe-Heitler process.

- On the forward proton side, a neutron spectrometer is required. A dipole magnet bends the hadron beam away from the collision axis to provide space for this element. It also generates dispersion which helps to detect forward scattered protons in detectors that are integrated into the hadron beam pipe, called "Roman Pots".

Figure 5 shows a schematic of the top-view of the IR with 22 mrad beam crossing angle which satisfies all these conditions. For high luminosities, the β-functions at the IP are required to be as small as possible. In the case of 10 GeV electrons colliding with 275 GeV hadrons, the β-functions are $\beta^*_{x,e} = 42$ cm, $\beta^*_{y.e} = 5$ cm, $\beta^*_{x,p} = 90$ cm, and $\beta^*_{y,p} = 4$ cm (see Table 1).

To avoid generation of an excessive amount of chromaticity in the low-β quadrupoles, these magnets should be placed as close as possible to the interaction point. Special quadrupole magnets are needed to focus the two beams with the conditions and constraints mentioned above.

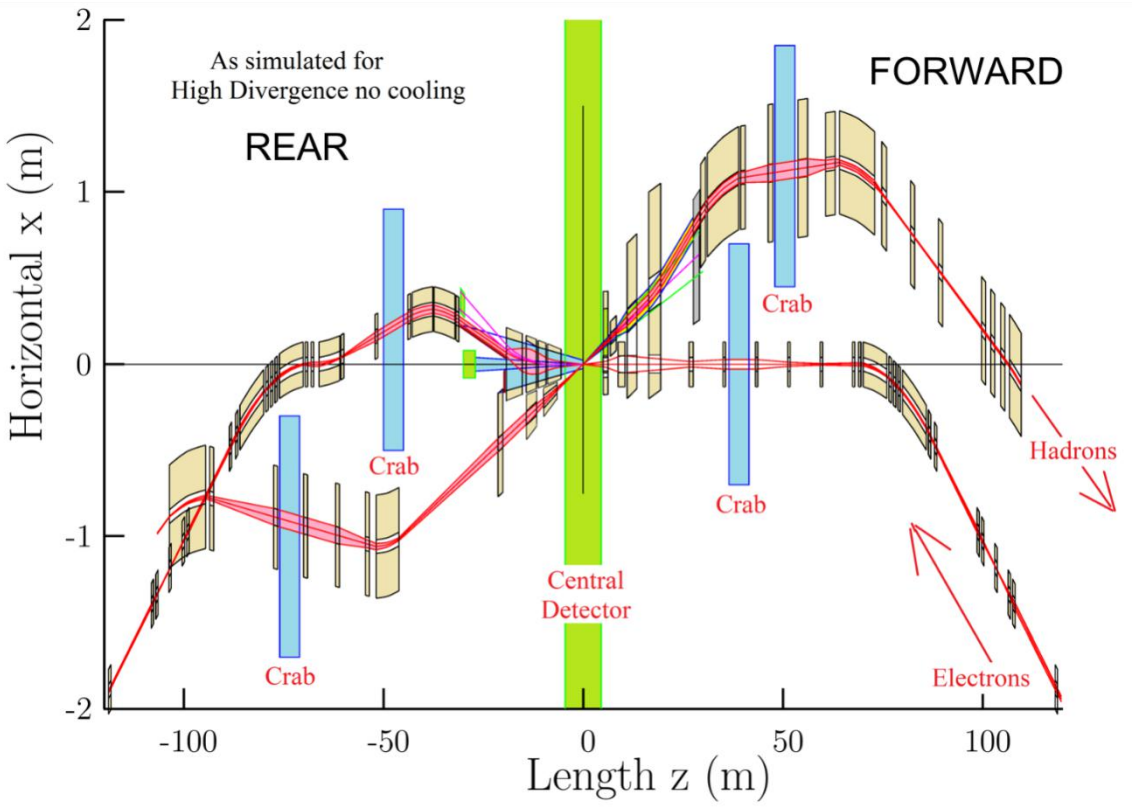

Figure 5: Schematic layout of the interaction region (top view). Beams cross at an angle of 22 mrad. Note that the length scales for the horizontal and vertical axis are very different. The IR design integrates focusing magnets for both beams, luminosity and neutron detectors, electron taggers, spectrometer magnets, near-beam detectors (Roman pots for hadrons), crab cavities, and spin rotators for both beams. The two beams are focused by quadrupole doublets. On the hadron-forward side, there are separate focusing magnets which are longitudinally interleaved. The first quadrupole magnet for electrons is integrated into a hadron spectrometer dipole. On the rear side, hadrons and electrons are focused by quadrupoles which are installed side-by-side in the same cryostat. The maximum β-functions in the IR for hadrons of 1600 m remain within the operating range of RHIC, while the maximum β-functions for electrons remain below 400m.

On the forward side, electron and hadron quadrupole magnets are interleaved. The first magnet is a room temperature spectrometer magnet with a very large aperture which is large enough for the first quadrupoles for the electron beam. The electron beam is shielded from the strong fields of the superconducting hadron quadrupoles by either active shielding coils (1st hadron quadrupole) or by a strong return yoke with a cut-out for the electron beam (2nd hadron quadrupole). A strong dipole magnet is required on this side of the IP to steer the hadron beam away from the path of neutrons that are detected in the downstream neutron detector placed in this area as well.

On the rear side, the superconducting focusing magnets for electrons and protons are installed side-by-side in the same cryostat. A steel return yoke shields the electron beam from the field of the hadron quadrupole magnets. Electron quadrupoles have an extra large aperture to provide sufficient space for the synchrotron radiation fan which is generated by the forward-side quadrupoles and must be absorbed further downstream,

far away from sensitive detector components. The electron beam is steered away from the path of γ-radiation created by electron-hadron scattering (Bethe-Heitler), which is used to measure luminosity. The bending magnet acts as a spectrometer magnet for the electrons which lost energy in the Bethe-Heitler process. These are tagged as part of the luminosity measurement.

The positions of all these IR-magnets are shown in Figure 5. The cross-section of the first quadrupoles on the hadron-rear side is shown in Figure 6. The properties of the IR quadrupoles are summarized in Table 3.

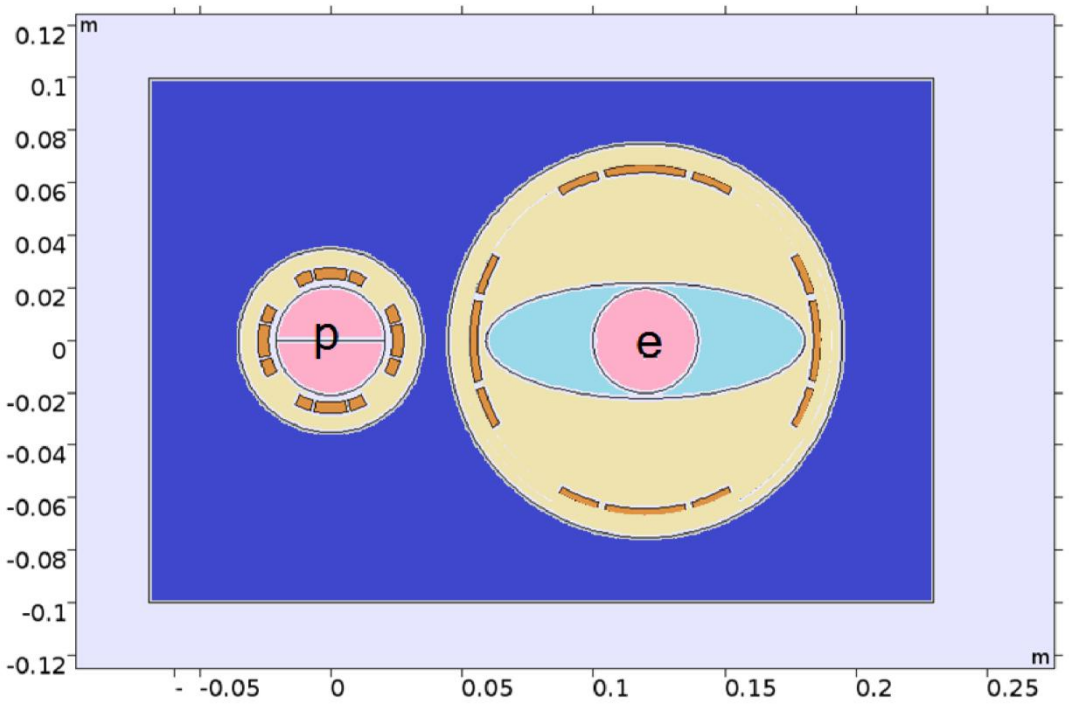

Figure 6: Cross section through the first low-β quadrupole cryostat on the hadron rear side (electron forward side). The two superconducting magnets, one for hadrons (left) and one for electrons (right) are separated by a common return yoke structure

Table 3: Summary of IR superconducting (s.c.) and normal-conducting (n.c.) magnets.

Hadron Forward Side

Name	*Beam*	*Position entrance [m]*	*Length [m]*	*Strength*	*Aperture entrance [mm]*	*Aperture exit [mm]*	*Coil*
B0	hadrons	5.0	1.2	1.3 T	500x240	500x240	s.c. NbTi
Q0FE	electrons	5.0	1.2	14.6 T/m	22	22	s.c. NbTi
Q1FP	hadrons	6.8	1.5	131 T/m	84	84	s.c. Nb_3Sn
Q1FP shield	electrons	6.8	1.5	N/A	N/A	N/A	s.c. NbTi
Q1FE	electrons	8.74	1.72	6.0 T/m	48.5	48.5	s.c. NbTi
Q2FE	hadrons	11.1	2.4	45 T/m	210	210	s.c. NbTi
B1	hadrons	13.9	3.0	4.47 T	270	1270	s.c. NbTi

Hadron Rear Side

Name	*Beam*	*Position [m]*	*Length [m]*	*Strength*	*Aperture entrance [mm]*	*Aperture exit [mm]*	*Coil*
Q1RE	electrons	5.5	3.42	5.1 T/m	135	186	s.c. NbTi
Q1RP	hadrons	5.5	3.42	82.9 T/m	42	86	s.c. NbTi
Q2RE	electrons	11.67	2.57	4.23 T/m	228	266	s.c. NbTi
Q2RP	hadrons	11.67	2.57	54.86 T/m	90	110	s.c. NbTi
BER1	electrons	19.2	4.0	0.09 T	281	338	s.c. NbTi

The maximum β in the low-β quadrupoles for protons are $\beta_{xp} = 1600\,\mathrm{m}$ and $\beta_{yp} = 1200\,\mathrm{m}$, respectively. For electrons the corresponding numbers are $\beta_{xe} = 1000\,\mathrm{m}$ and $\beta_{ye} = 200\,\mathrm{m}$.

The two beam lines are relatively close, so the early magnets of both beams need to have limited outside radial dimensions, outside of which the fields must be low. The magnets on the forward side use active shielding as demonstrated at BNL for an ILC IR application [10], or in the case of the dipole B1, a yoke with a hole in it for electrons. The apertures for the hadron magnets are considerably larger than required by the circulating hadron beam to provide sufficient clearance for scattered hadrons from the IP to be detected further downstream.

2.2.7 **Spin Rotators**

Spin polarization of the electron beam is preserved in beam storage if the spin orientation in the arcs of the accelerator is vertical. In collision, both electron and proton spins are required to be in the longitudinal direction. In order to rotate the electron spin from the vertical direction in the arcs to the longitudinal direction, a set of magnets called spin rotators are required and need to be integrated into the interaction region. A second spin rotator which rotates the spin back into the vertical direction is required after the beam passes the interaction point. Spin rotators are an integral part of the interaction region and are associated with a number of beam optics conditions which are discussed below.

The proton spin rotators are identical to the ones presently used in RHIC, which are based on helical dipole magnets. Spin rotators based on helical magnets have been successfully used for polarized protons in RHIC [11][12].

A helical magnet design leads to smaller orbit excursion compared with a design based on regular dipoles. The eRHIC electron spin rotators must operate over a large energy range, from 5 GeV to 18 GeV. Since the orbit excursion in the dipole magnets (either regular or helical) scales inversely with the beam energy, a HERA-type rotator leads to 1 m orbit excursions of 5 GeV electrons [13].

Furthermore, the synchrotron radiation power per meter produced by 18 GeV eRHIC electrons is considerably larger than that generated by the 27.5 GeV electrons in HERA due to the much larger electron current. Reducing the linear power load requires further increasing the rotator length and, correspondingly, the orbit excursion. Therefore, the most practical solution consists of a spin rotator based on strong solenoid magnets. Solenoidal Siberian Snakes have been used in electron accelerators operating in the 0.5 GeV to 1 GeV range [14].

The spin rotators for electrons are based on interleaved solenoids and bending magnets. Figure 7 depicts a schematic of the locations of all components around the interaction region. Light green boxes represent solenoidal magnets of the spin rotators. Blue lines and blue boxes are normal quadrupoles and dipole bending magnets, respectively. Each of the long and short solenoid modules contains a solenoid (split into two half-sections), and seven normal quadrupoles that compensate the impact of the strong solenoidal fields on beam optics and transverse coupling and satisfy the required spin matching conditions. The lengths of the solenoids are chosen such that the maximum magnetic field required is 7 T. The settings for the magnetic fields of the solenoids to achieve longitudinal polarization of the electron beam depend on the beam energy. Optimization of the solenoidal spin integrals led to the parameters listed in Table 4.

The optics functions through the IR are shown in Figure 8. The set of β-functions describing this coupled case is given in Mais-Ripken parameterization [15]. Betatron coupling functions are limited to the rotator insertions, which are also dispersion-free.

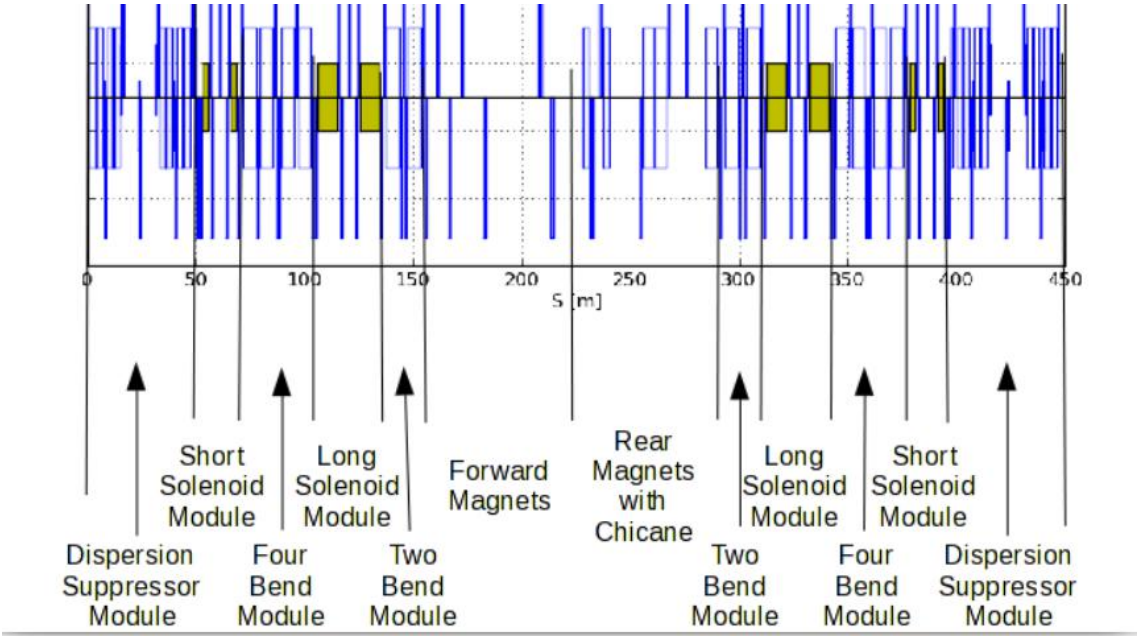

Figure 7: Major components of the electron lattice around the interaction region. Spin rotator magnets are shown as green boxes. The blue boxes indicate quadrupole and dipole magnets

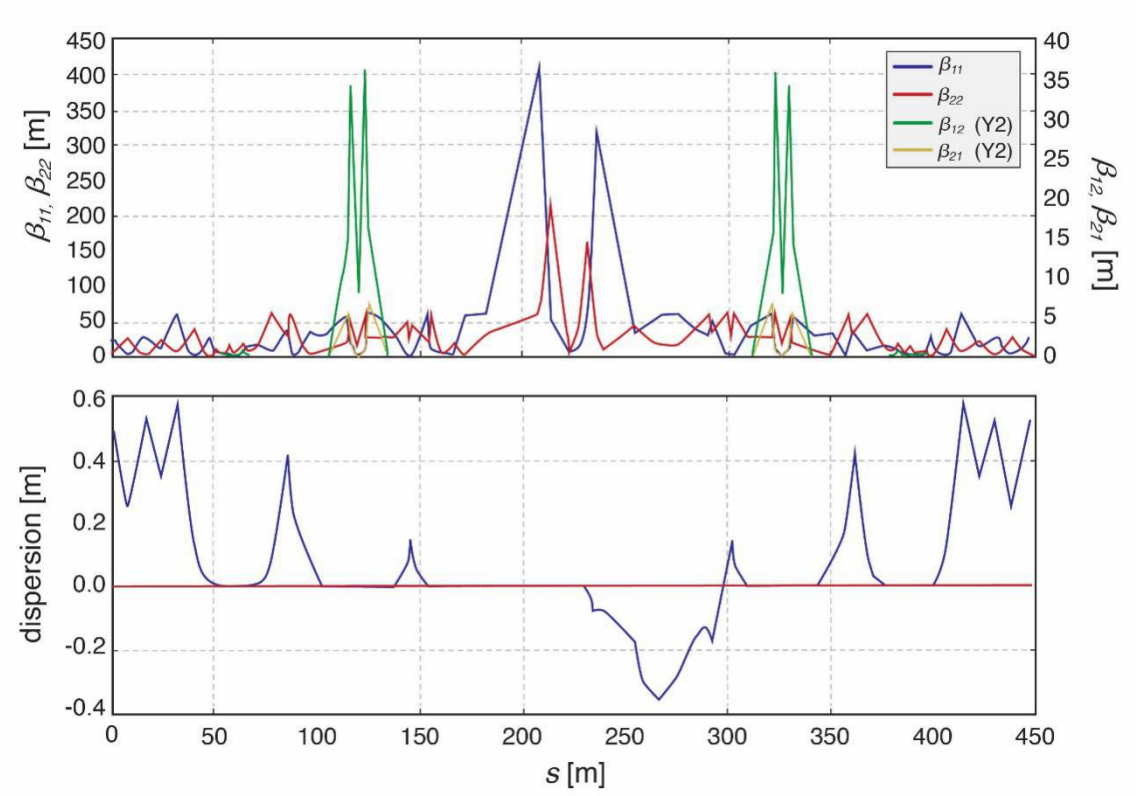

Figure 8: 18 GeV electron beam optics in the colliding straight section with the interaction region, the matching sections, the spin rotators, and dispersion suppressors. In the center of the plot is the interaction point (IP) with large values of the β-functions on both sides. The additional β peaks, denoted by $\beta_{1,2}$ and $\beta_{2,1}$ in this plot are caused by the coupled β-functions which vanish outside the rotator. These are drawn on a different scale shown on the right-hand side of the plot

Table 4: Spin rotator parameters.

Parameter	*Short solenoid module*	*Long solenoid module*
Field integral range [T-m]	20-34	4-122
Solenoid length [m]	5.4	18.
Solenoid spin rotation angle (at 18 GeV)	32°	116°
Location in the RHIC tunnel	D9-D10	D6-Q8

2.2.8 Electron Storage Ring

2.2.8.1 *Electron Storage Ring Overview*

The electron storage ring is located in the existing RHIC tunnel, in the same plane as the ion ring, and has a circumference of 3833.940 m which matches the proton revolution time at 133 GeV, an energy that balances the orbit offsets required for maintaining the revolution time at 100 GeV and 275 GeV. Like the ion ring, it consists of alternating inner and outer arcs in order to have the same revolution time as the ion ring. With the existing Yellow Ring of RHIC being used as the eRHIC ion ring, the

electron ring will be placed on the opposite side, the side of the Blue ring, as illustrated in Figure 9.

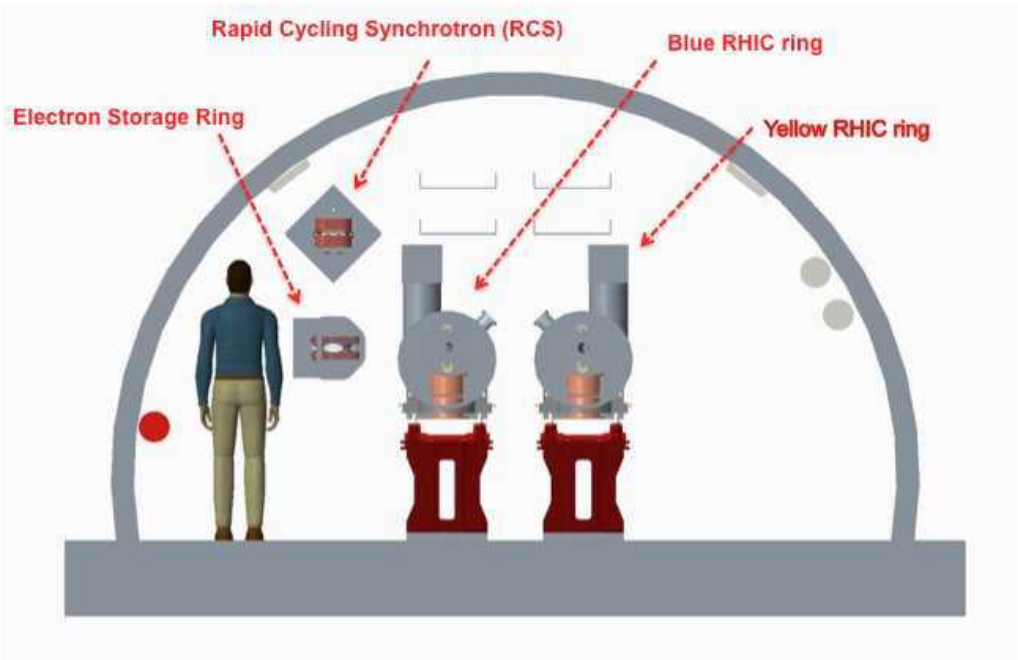

Figure 9: Location of the electron storage ring in the tunnel arcs, on the opposite side of the Blue ring. The Rapid Cycling Synchrotron injector is mounted above the collider ring plane

As in the present RHIC, there are six arcs separated by six ~200 m long straight sections with a potential interaction point (IP) in the middle. The IPs are denoted by their geographical positions as 2 o'clock to 12 o'clock, with 12 o'clock being in the North.

The ring is organized as follows:

Straight section IR6: colliding beam detector with hadron/electron low-β section, spin rotators and crab cavities;

Straight section IR10: superconducting RF systems, strong hadron cooler facility, hadron beam abort;

Straight section IR12: damper systems, special instrumentation, electron injection/extraction;

Straight section IR2: electron source and pre-injector LINAC;

Straight section IR4: half of the superconducting RF systems, hadron injection, hadron RF;

Straight section IR8: 2nd colliding beam detector, spin rotators and crab cavities.

The average arc radius is 381 m, while the actual dipole bending radius is $\rho = 242$ m. The lattice in the arcs and the non-colliding utility straights is composed of FODO cells.

Each of the main dipoles in the arcs consists of three individual bending magnets, a short, 0.445 m long magnet in the center between two longer (l = 2.66 m) magnets.

In this configuration, the amount of synchrotron radiation can be controlled to ensure sufficient radiation damping for all beam energies between 5 and 18 GeV, thereby providing sufficient damping decrements in support of strong beam-beam parameters of

$\xi_{x,y} \leq 0.1$ (see below).

Simultaneously, the split magnets produce the desired beam emittance at the 5 GeV beam energy. Each arc of the electron ring is composed of 16 identical FODO cells. Each half cell consists of a 0.6 m long quadrupole, a 0.5 m long sextupole, a 6.06 m long dipole triplet, and a 0.25 m long dipole corrector. The drift spaces between the individual magnets are slightly different for the inner and outer arcs to account for the difference in the average bending radius. Figure 10 shows the layout of one arc FODO cell.

At both ends of each arc, two additional FODO cells with individually powered quadrupoles are used to match the optical functions between the straights and the arc, and to suppress the dispersion in the straight sections. A missing-magnet scheme eases the dispersion matching.

The specific horizontal emittances required at different energies are realized by a combination of FODO cell phase advances in the arc, and utilizing the super-bends, while the vertical emittance is controlled by applying a vertical dispersion bump. At a beam energy of 18 GeV, the phase advance per arc FODO cell is set to 90 degrees, while at 5 and 10 GeV it is reduced to 60 degrees. The vertical phase advance is set to the same value in order to maximize the dynamic aperture. These different phase advances require a flexible chromaticity correction scheme, based on four families for a FODO cell phase advance of 90 degrees, and 6 families for a 60 degree phase advance. The parameters of the beam optics of the arcs for different beam energies are shown in Table 5.

Table 5: Parameters of the electron beam optics in the arcs for different beam energies. At the lowest energies $E < 10$ GeV, the short dipole in each half-cell is reversed, thus creating a super-bend. This increases radiation damping and damping decrement, provides the required beam emittances, and avoids the bunch length becoming too short.

Energy [GeV]	***5***	***10***	***18***
Phase advance per cell [degrees]	60	60	90
Horizontal emittance [nm]	20	20	22
Relative energy spread [10^{-4}]	5.8	5.5	10.0
Transverse damping time [turns]	7750	5450	940
Natural chromaticity x/y [turns]	-96.2/-89.5	-96.2/-89.5	-101.2/-99.6
Momentum compaction factor [10^{-3}]	1.03	1.04	0.53
Quadrupole strength k_{QF} [m^{-2}]	0.215	0.215	0.283
Quadrupole strength k_{QD} [m^{-2}]	0.216	0.216	0.279
Number of sextupole families	6×2×3	6×2×3	6×2×2
Arc β_{xmax} [m]	27.7	27.7	26.5
Arc β_{ymax} [m]	27.4	27.4	26.8
Arc maximum dispersion [m]	0.95	0.95	0.57
Quadrupole aperture requirement x/y [mm]	30/30	30/30	30/30

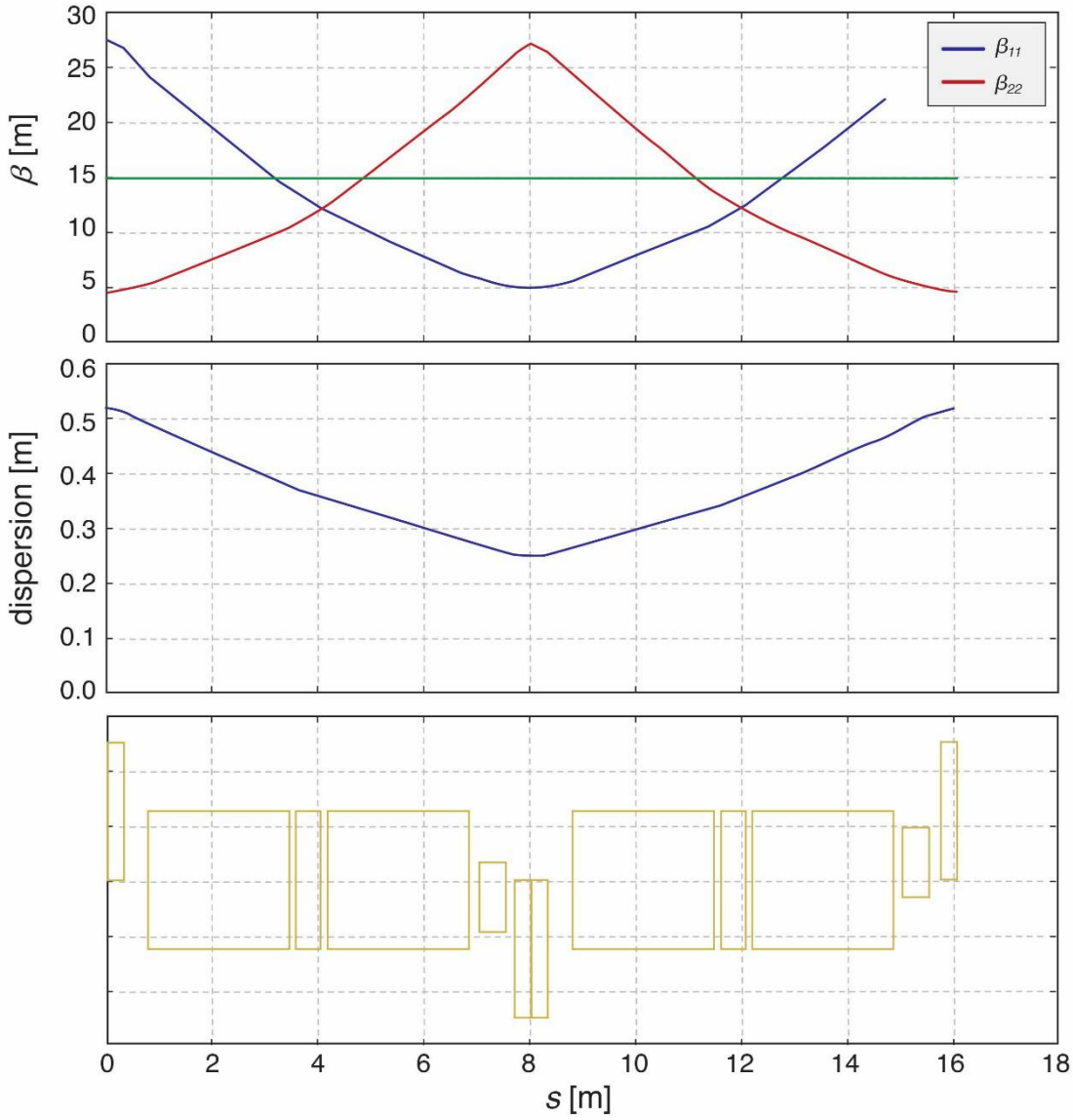

Figure 10: One arc FODO cell for an outer arc cell. The lengths of individual components are to scale.

the arcs. The small β-functions at the IP result in large β-functions in the low-β quadrupoles.

The horizontal β-functions are intentionally large at the crab cavities in order to lower the required cavity voltage. Together with the large β-functions in the final focus quadrupoles, these contribute significantly to the chromaticity. The solenoid spin rotators induce betatron coupling. This coupling is compensated by splitting each solenoid into two individual magnets with a system of five individually powered quadrupoles between them. Spin matching is accomplished by adjusting 40 independent quadrupole circuits in the interaction region. Figure 7 shows the colliding straight section with the interaction region, matching section, dispersion suppressors, and spin rotators.

2.2.8.2 *Maintaining Radiation Damping and Emittance Control for 5 GeV Electron Beams*

Radiation damping allows the electron beam to have a large beam-beam tune shift. While sufficient radiation to allow a large beam-beam tune shift is produced at higher energies, simply scaling down the dipole fields for lower energies does not result in sufficient radiation damping to allow for the same large beam-beam tune shift. The radiation damping for 11 GeV still corresponds to the damping decrement $\delta = 1/(f_c \tau_{x,y})$ of KEKB, where $\tau_{x,y}$ denotes the horizontal and vertical damping time, while f_c is the revolution frequency.

The solution to this is to place three dipoles, instead of a single dipole, between the arc quadrupoles. At high energies (18 GeV), all three dipoles have the same field. At the lowest energy (5 GeV), the central dipole will have a higher field (0.46 T) and reversed polarity. This will increase synchrotron radiation sufficiently to reduce the transverse damping times to 50 ms which gives a damping decrement comparable to that realized in KEKB. This arrangement will also increase the beam emittance close to the 10 GeV value whereas the total synchrotron radiation power is less than half the 10 GeV value (3.2 MW). Figure 11 shows schematically the dipole configuration and orbits at different energies.

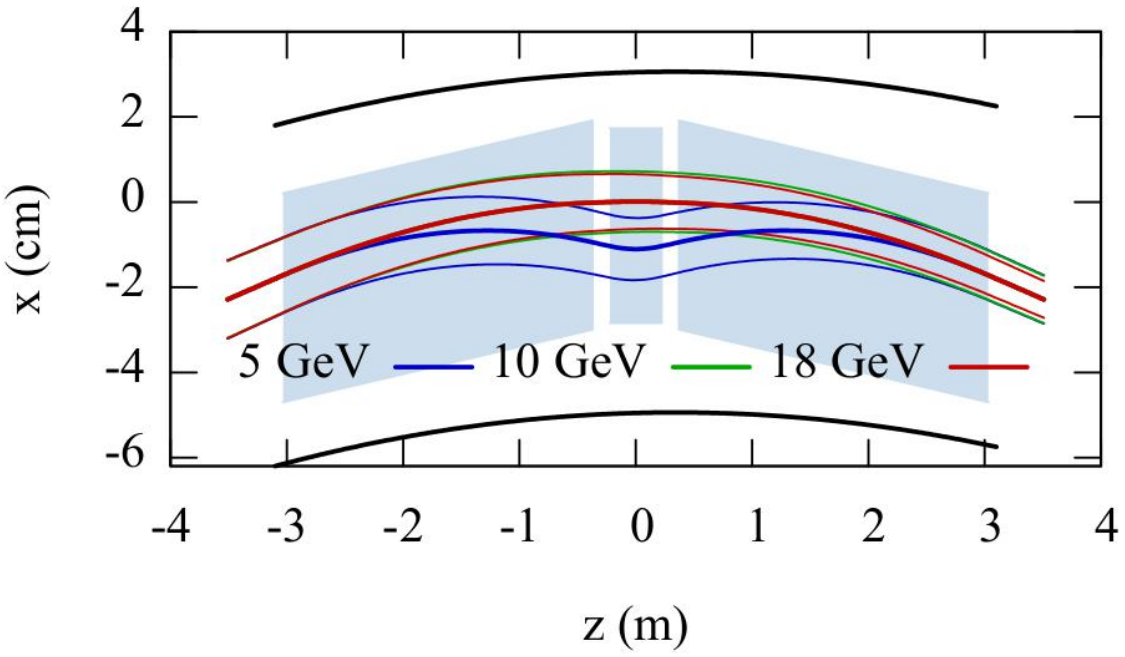

Figure 11: Schematic view of beam orbits in the split dipole magnets for various beam energies

There are three impacts associated with this scheme:

- Higher dipole fields are required;
- The orbits are different for each energy, requiring wider dipoles and a wider vacuum chamber;
- The additional drifts between dipoles reduce the dipole packing fraction, leading to unwanted higher synchrotron radiation losses at higher energies.

The parameters of the electron storage ring are summarized in Table 6.

Table 6: Parameters of the Electron Ring Lattice.

Parameter	*Value*
Path length in dipoles per half-cell [m]	6.06
Bend angle [mrad]	23.8
Number of split dipoles in the entire ring	252
Drift space between split dipoles [m]	0.15
Transverse Damping decrement	$(1.3 - 10.6) \times 10^{-4}$
Minimum Beam Energy [GeV]	5
Length of strong center dipole [m]	0.45
Field strength of center dipole [T] at 5GeV, 18GeV	-0.456, 0.248
Max. Difference between 5GeV and 18GeV orbits [mm]	14
Length of weak and long dipole [m]	2.66
Field strength of center dipole [T] at 5GeV, 18GeV	0.113, 0.248

2.2.8.3 *Electron Spin Polarization in the Storage Ring*

The collision of longitudinally polarized electrons and ions is a key requirement of an electron-ion collider, and a large effort has been undertaken to ensure good polarization of the electron beam during the store. The evolution of beam polarization in electron storage rings is defined by two processes related to synchrotron radiation: Sokolov-Ternov self-polarization [2], and depolarization caused by stochastic photon emission [17]. The self-polarization process leads to a build-up of electron polarization in the direction opposite to the vertical guiding field, up to a maximum level of 92.4% in a perfectly planar storage ring without spin rotators. Stochastic photon emission leads to a randomization of the particle spin directions (spin diffusion) and reduces the equilibrium polarization level.

Because experimenters call for the simultaneous storage of electron bunches with both spin helicities, the Sokolov-Ternov effect is not an option for eRHIC as it tends to polarize
all bunches in the same direction. A full energy polarized electron injector is needed instead, so that the electron bunches are injected into the storage ring with high transverse
polarization (~85%) and the desired spin direction.

In the storage ring the polarization is then brought into the longitudinal direction at the IP
by a pair of solenoidal spin rotators.

The self-polarization rate has a strong dependence on beam energy (as γ^5) and dipole bending radius (as $<1/|\rho|^3>$). The self-polarization time for the eRHIC storage ring placed in the present RHIC tunnel is shown in Figure 12. It takes into account the split dipole structure which enhances the synchrotron radiation at energies below 10 GeV. The self-polarization time is quite long over the entire energy range, except when approaching 18 GeV where it drops to about 30 minutes.

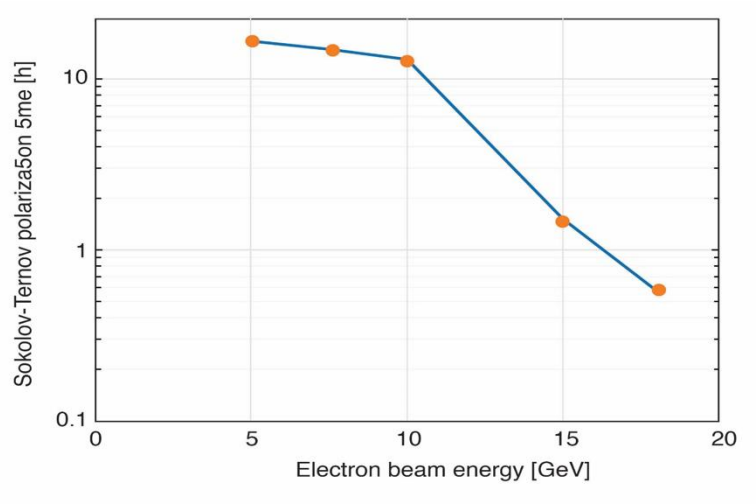

Figure 12: Sokolov-Ternov electron spin polarization time as a function of electron beam energy. The depolarization for spin parallel to the magnetic guide field due to the Sokolov-Ternov effect becomes important for beam energies well above 10 GeV.

While the Sokolov-Ternov effect is a slow process, stochastic photon emission in the storage ring in the presence of misalignments and spin rotators may quickly destroy the polarization of the injected beam, thus requiring a continuous replacement of the depolarized bunches. Spin matching is needed in order to minimize the spin diffusion introduced by the rotators. For the eRHIC storage ring, as the vertical dispersion vanishes at all bending magnets, it is sufficient and necessary to provide spin matching only for horizontal and synchrotron motion between the rotator pairs, by using the quadrupoles interleaved with the rotator solenoids.
We may assess the requirement on polarization in the eRHIC storage ring by considering that polarization varies with time as

$$P(t) = P_{\infty}\,[1 - \exp(-t/\tau_p)\,] + P(0)\exp(-t/\tau_p) \qquad (4)$$

where $P(0)$ is the starting polarization and P_{∞} and $1/\tau_p$ are the actual asymptotic polarization and polarization rate respectively.
It holds

$$P_{\infty} \cong \frac{\tau_p}{\tau_{BKS}}\, P_{BKS} \qquad \frac{1}{\tau_p} \cong \frac{1}{\tau_{BKS}} + \frac{1}{\tau_d} \qquad (5)$$

where $1/\tau_d$ is the spin diffusion rate, P_{BKS} and $1/\tau_{BKS}$ are respectively the asymptotic polarization and the polarization rate for the ideal machine in absence of spin diffusion (the Baier-Katkov-Strakhovenko [26] generalization of Sokolov-Ternov quantities for a lattice where the magnetic field is not homogenously vertical). Equations (4) and (5) can be used for evaluating the polarization evolution with time for

bunches polarized parallel or anti-parallel to the bending field. Fig.12a shows the polarization evolution for eRHIC storage ring at 18 GeV for $P(0)$=+85% (anti-parallel) and -85% (parallel) with P_∞ =30% and 50%.

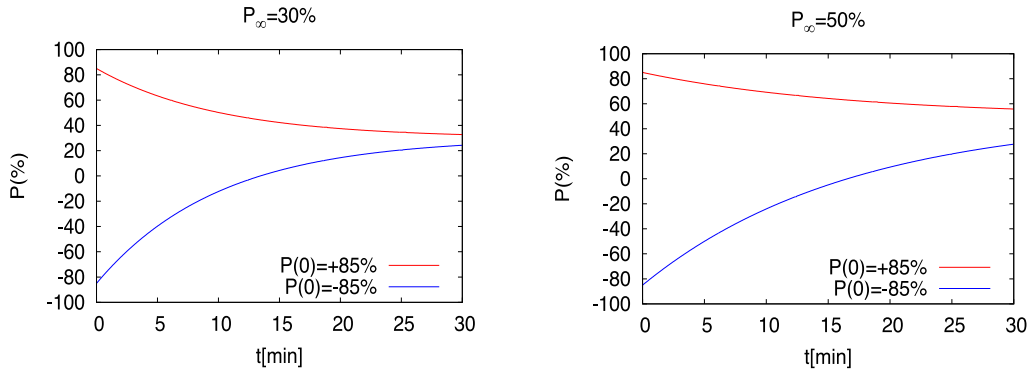

Figure 12a: Polarization vs. time for bunches with starting polarization anti-parallel to the bending field ($P(0)$=+85%) and parallel to it ($P(0)$=-85%) when the ring asymptotic polarization is 30% (left) and 50% (right).

Fig.12b shows polarization after 5 minutes from injection and the 5 minutes average polarization vs. P_∞ with $P(0)$=-85%. The benefit of increasing P_∞ saturates above ≈50% for the bunches with initial polarization parallel to the guiding field.

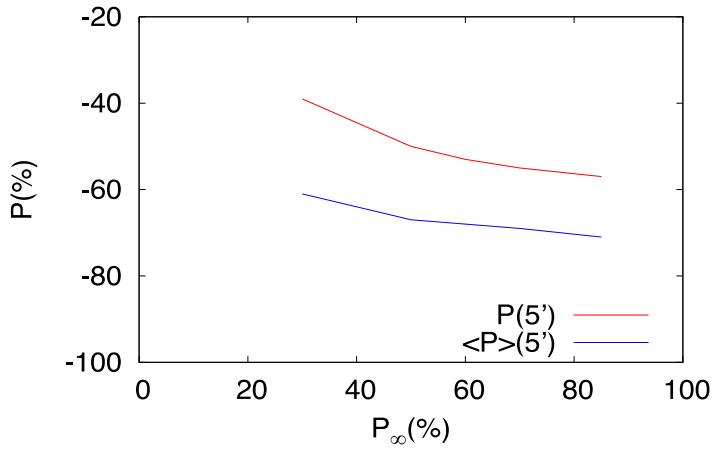

Figure 12b: Polarization after 5 minutes vs. P_∞ for bunches with starting polarization parallel to the guiding field ($P(0)$=-85%) (red). Its average over 5 minutes vs. P_∞ .

For polarization computations in the eRHIC storage ring we rely at the moment on the SITROS package [27]. SITROS includes a module, SITF, where orbit and spin motion are linearized, and a Monte-Carlo tracking module with 2nd order orbital motion and non-linear spin motion in the presence of quantum excitation and radiation damping.

Once the 6D equilibrium distribution is reached, to each particle a spin is added aligned to the stable polarization direction, namely the periodic solution of the Thomas-BMT equation [28][29], and tracking is pursued over an additional number of turns chosen by the user. Depolarization rate and asymptotic polarization are evaluated from the fit of $P(t)$. The fully 6D code SITF reads the same input file allowing preliminary checks before embarking on time consuming tracking. SITROS has been developed for PETRA and HERA-e and improved in view of the HERA luminosity upgrade. SITROS results for HERA-e were in good agreement with observations, with the exception of the evaluation of beam-beam interaction effects which appeared to be somewhat pessimistic. For the moment the polarization studies have been limited to the 18 GeV case, which is expected to be the most challenging one. The machine tunes are set to Q_x =0.12, Q_y =0.10 and Q_s =0.046 for luminosity operation. It is important to show that an asymptotic polarization ≥50% can be achieved also in presence of misalignments.

2.2.8.4 *Polarization in the unperturbed ring*

Fig.12c shows the asymptotic polarization vs. the "naive" spin tune $a\gamma$, a = 0.0011596 being the electron gyromagnetic anomaly, for the unperturbed ring in linear spin motion approximation and as results from the tracking. It can be expected that, manifesting the presence of higher order resonances and synchrotron side-bands, tracking calculations give lower polarization than calculations with linearized spin motion. However the discrepancy seems exceedingly large in this case. This may be related to the fact that the vertical emittance as computed by the tracking is about 8 times larger than expected, or to the fact that the IR optics is not yet fully spin matched.

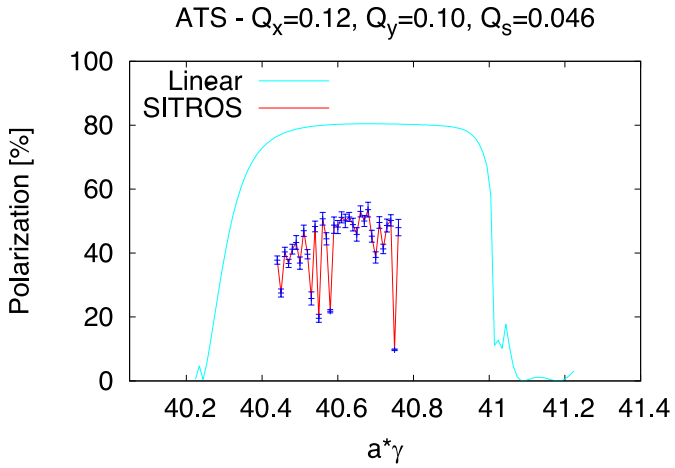

Figure 12c: Polarization vs. $a\gamma$ for the unperturbed ring in linear spin motion approximation (cyan) and as results from the tracking (red).

Fig.12d shows the RMS deviation from the vertical direction in the machine arcs of the

periodic solution to the Thomas-BMT equation, $\hat{n}_0$, which is vertical in the arcs and longitudinal between the rotator pair.

Although the solenoid strength is kept fixed, the deviation is small in the energy range considered.

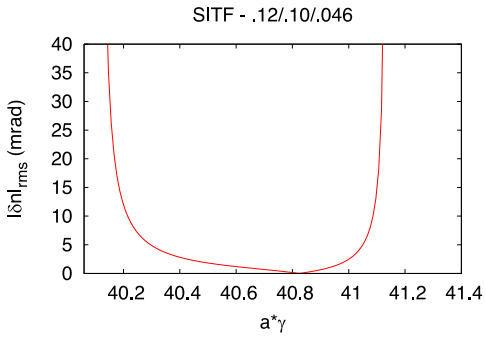

Figure 12d: RMS $|\delta\hat{n}_0|$ vs. $a\gamma$ for the unperturbed ring.

2.2.8.5 *Polarization in presence of misalignments*

Key points to achieve high polarization are the optimization of the betatron tunes, a well corrected closed orbit and a dedicated correction of $|\delta\hat{n}_0|$.
Following simulations are based on the MAD-X misalignment/correction tool kit. The resulting optics is dumped into a file which can be read by the SITROS package. 494 Beam Position Monitors (BPMs), measuring the beam position in both planes, have been added close to each quadrupole together with 494 vertical and 494 horizontal correctors. The RMS values of the quadrupole misalignment assumed are δx=δy=200 μm and a roll angle $\delta\Psi$=200 μrad. BPMs errors have not been included yet. It turns out that due to the large coupling in the solenoid sections, the orbit cannot be corrected in a satisfactory manner in the two planes separately in the whole machine as done by the MAD-X correction module. One way out was correcting both planes simultaneously with an “external" code and reading back the corrections with MAD-X. 46 independently powered skew quadrupoles, inserted at high D_x β_y and β_x β_y locations, are used for correcting spurious vertical dispersion and betatron coupling which are large due to the vicinity of the working point to the linear coupling difference resonance. Figs.12e and 12f show polarization for a particular error realization after closed orbit correction and with vertical dispersion and betatron coupling correction in addition respectively.

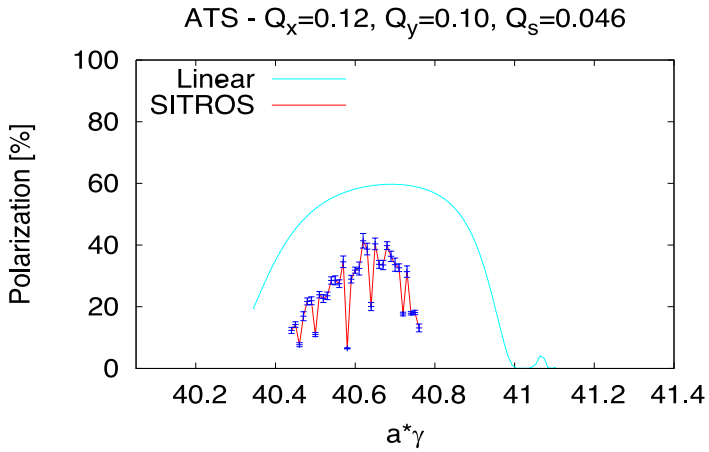

Figure 12e: Polarization vs. $a\gamma$ for the perturbed ring after closed orbit correction in linear spin motion approximation (cyan) and from tracking (red).

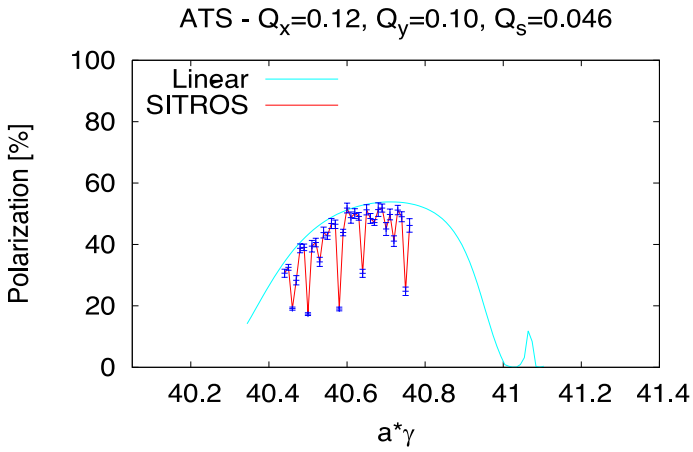

Figure 12f: Polarization vs. $a\gamma$ for the perturbed ring after closed orbit correction and skew quadrupoles optimization, linear spin motion approximation (cyan) and from tracking (red).

The deviation of the actual $\hat{n}_0$ on the perturbed orbit wrt to the nominal direction can be corrected resorting to *harmonic bumps* as done at HERAe [30] and LEP [18]. Fig.12g shows the RMS value of $|\delta\hat{n}_0|$ vs. $a\gamma$ before and after correction by harmonic bumps. Fig.12h shows the resulting polarization.

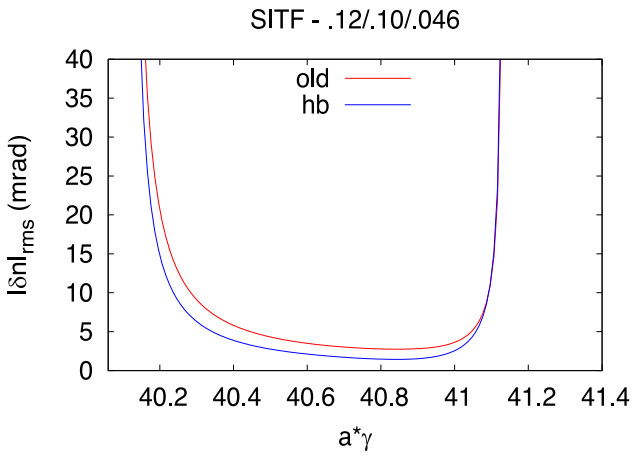

Figure 12g: RMS $|\delta \hat{n}_0|$ vs. $a\gamma$ for the the perturbed ring before (red) and after (blue) harmonic bumps optimization.

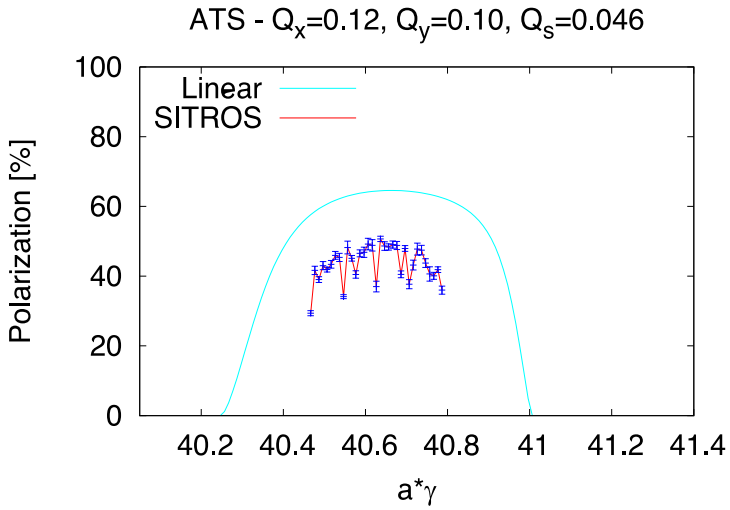

Figure 12h: Polarization vs. $a\gamma$ for the perturbed ring after closed orbit correction, skew quadrupoles optimization and $|\delta \hat{n}_0|$ correction. Cyan: linear spin motion approximation; red: tracking.

2.2.8.6 *Further considerations*

As discussed above, the eRHIC storage ring uses split dipoles to increase the damping decrement at lower energies. Such enhanced synchrotron radiation increases the spin diffusion rate. Thus, attention must be paid to the possibility of enhanced depolarization at lower energies too.

Similarly, the effect of beam-beam interactions on polarization requires consideration. The counter-rotating proton beam perturbs the electrons orbital and spin motion and acts as a non-linear focusing lens which shifts the beam tune and increases the tune spread, in particular in the vertical plane. The shift can be obviously compensated by the tuning quadrupoles; however the increased spread may affect the lifetime of the beam tails and restrict the tuning range. Running below the integer (*mirror tunes*) could ease the problem.

In HERA-I with one pair of spin rotators and $\xi_y^e \approx 0.06$ for two IPs, the effect of beam-beam interactions on polarization was not critical and with careful tuning beam polarization between 50% and 60% was delivered. Beam-beam effects however were clearly visible. For instance it was observed that non-colliding positron bunches could have a smaller polarization in collision mode because the tunes were optimized for colliding bunches. As a consequence of the removal of the experiment solenoid compensators and the introduction of 2 more spin rotators, in HERA-II the expected polarization was about 60% [16], w/o beam-beam effects. In addition ξ_y^e increased up to about 0.09. With positrons, for which the proton beam acts as a defocusing lens, the delivered polarization during collision was between 40% and 50%. With electrons however polarization reached only 30%-40% which increased to 40%-50% as for positrons, by operating the machine with mirror tunes.

The beam-beam tune spread might push a significant part of the eRHIC electrons away from ideal tunes for good polarization. However a state of the art orbit correction and a more efficient polarimeter are expected to increase the achievable polarization also in presence of beam-beam.

2.2.8.7 *Electron Storage Ring Dynamic Aperture*

The dynamic aperture of the electron storage ring is critical; the interaction regions contribute with maximum functions of ~400 m approximately 30% per IP to the natural chromaticity. A phase advance of 90 degrees per FODO cell is required to achieve the desired horizontal beam emittance of 20 nm for *18* GeV beam energy. At 10 GeV, where the highest luminosity is achieved, the optimum betatron phase advance in the arcs is 60 degrees per FODO cell. The total natural chromaticity including one IR is $\xi_{x,y} \cong -97.3, -92.4$. At 18 *GeV*, the interaction region contributes chromaticities of $\xi_{x,y}^{IR} \cong -33, -25$.

The dynamic aperture for particles with an ideal value of momentum is maximized by using a two-family sextupole correction scheme to control $\xi_{x,y} = +1$. However, the large off-momentum β-beat generated by the low-β quadrupole magnets causes a large nonlinear chromaticity which deteriorates the off-momentum dynamic aperture.

The strategy to recover off momentum dynamic aperture is two-fold:

- Achieve as much intrinsic compensation of $(\Delta\beta_{x,y}/\beta_{x,y})/(\Delta p/p)$ by optimized betatron phase advances between the sources of chromaticity. However, this is constrained by the spin matching conditions and the special phase advances between crab cavities and IP.
- Arrange the sextupoles in the arcs in families tuned in order to create an off-momentum β-beat that cancels the off-momentum β-beat from the IR, while avoiding the generation of nonlinear resonance driving terms.

In addition, sextupoles in the dispersion-free straight sections, called "geometric sextupoles", may be used to minimize residual contributions to driving terms of nonlinear resonances.

The 6 eRHIC arcs, however, consist of 16 regular periodic FODO cells and have at each end three FODO cells for dispersion matching which are not identical to the regular cells.

For the 60 degree optics for a beam energy of 10 GeV, a scheme with a structure of 32 sextupole magnets (16 horizontally focusing and 16 vertically focusing ones) per arc is applied. These are powered in three horizontal and three vertical families, labelled by $A_{h,v}$, $B_{h,v}$, and $C_{h,v}$. Some of the possible sextupole positions are left empty (denoted by "*E*") which is the result of optimization. The scheme is:

A-B-E-A-B-A-B-C-A-B-C-A-B-E-A-B

Note that only horizontally focusing sextupoles are shown in this scheme. Vertically focusing sextupoles are interleaved with the horizontal ones; the scheme is the same. Sextupoles belonging to the same family are always spaced by 180 degrees. This implies that driving terms for off-momentum β-beat accumulate over the sextupoles of the same family and thereby maximize the potential for compensation of the β-beat from the IR. The contributions to nonlinear driving terms from sextupoles of the same family, however, cancel, so that non-linear effects are only created in higher orders. Since the β-beat generated in the IR arrives at each arc with a different phase, the sextupole families need to be re-optimized in each arc.

This scheme produces a dynamic aperture of $\pm 20\,\sigma_x$ and provides a momentum aperture of $\pm 7\ \sigma_E$. These values are believed to provide sufficient margin to accommodate magnetic imperfections and effects of misalignment.

An additional margin is provided by geometric sextupoles in the straight section, which have not yet been optimized. Figure 13 shows the on-momentum dynamic aperture in the x-y plane. The variation of tunes on a trajectory with a given starting point in phase space is used as a figure-of-merit for the stability of each point in phase space. The plot of such a frequency map [19] shows a clear border between stable and unstable motion.

The color code refers to the tune fluctuation $dQ = \log\left(\sqrt{\Delta Q_x^2 + \Delta Q_y^2}\right)$, where $\Delta Q_{x,y}$ are the differences in tune obtained by FFT over two successive periods of 1024 turns. Figure 14 shows the frequency map in the $x - \Delta p/p$-plane.

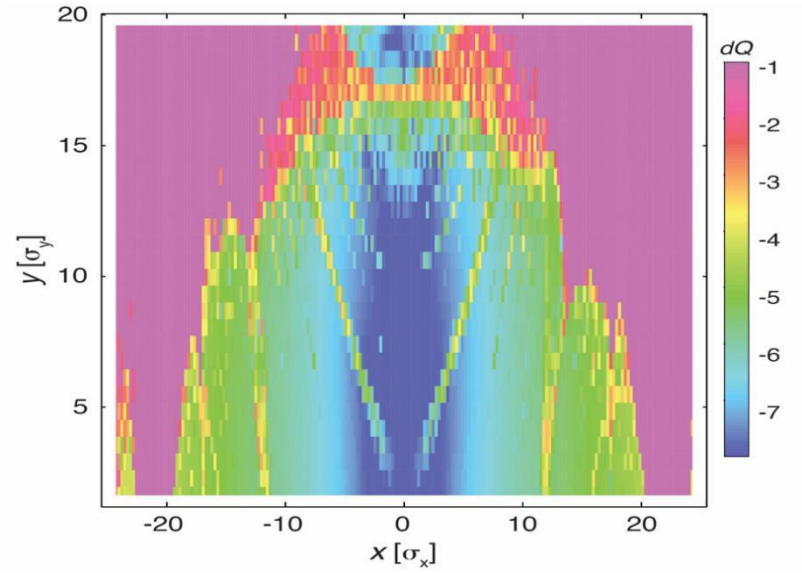

Figure 13: Frequency map of dynamic aperture in the *x-y* plane. The axis is plotted in units of RMS beam size at the starting point. The color scale (shown on the right-hand side) indicates the logarithm of tune fluctuations which are a measure for the stability of the motion

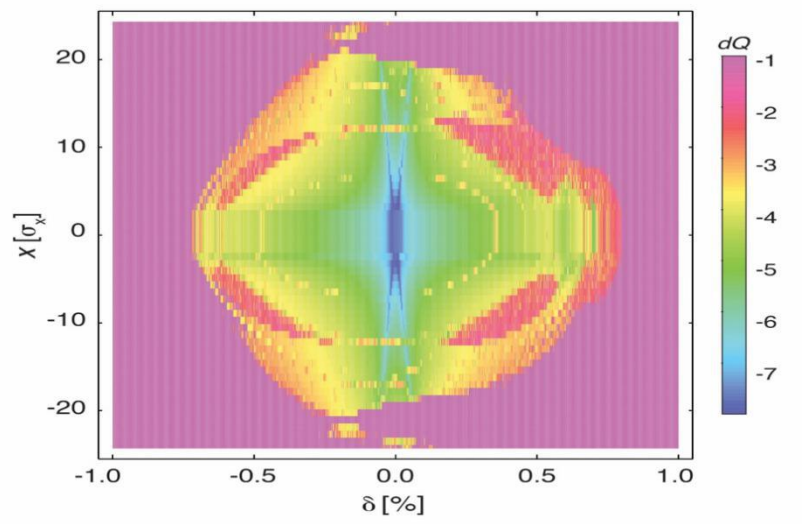

Figure 14: Frequency map of dynamic aperture in the *x-Δp/p* plane.

The beam optics for 18 GeV with a phase advance of 90 degrees requires a different strategy. With a phase advance of 90 degrees, two sextupoles in neighboring cells (horizontally focusing or vertically focusing, respectively) will generate an off-momentum β-beat if the two strengths are different. Sextupoles in successive cells with the same strength will add to this β-beat. However, there is no control over the phase of that β-beat. For this reason, the phase of the beat that originates at the IR needs to arrive with the correct phase at the first sextupole in the regular arc.

This requires the design of an appropriate betatron phase advance between the IP and the first sextupole in the arc. The betatron phase needs to be optimized between the 6 arcs in order to enable all sextupoles for correction of 2nd order chromaticity. Alternatively, one can arrange that the first arc corrects only the cosine-like part of the β-beat and the next arc, which would be spaced by a horizontal and vertical betatron phase difference from the first arc of $2(k+1)\pi/4$ (k integer), to correct the sine-like component of the β-beat (phase referring always to the first regular sextupole in the arc adjacent to the IR). The 18 GeV lattice is not fully optimized yet and is not further discussed. In case of unexpected difficulties, it will be possible to run with a 60 degree lattice at this energy which would result in some luminosity loss.

2.2.8.8 *Collective Effects in the eRHIC Electron Storage Ring*

We have considered coherent instabilities, intrabeam scattering and Touschek scattering.

Intrabeam scattering times in the electron storage ring are in the order of minutes, much longer than the 50 ms radiation damping times. Touschek lifetimes are hours, which is much longer than the bunch replacement time. We have considered coherent instabilities, intrabeam scattering and Touschek scattering.

Intrabeam scattering times in the electron storage ring are in the order of minutes, much longer than the 50 ms radiation damping times.

Touschek lifetimes are hours, which is much longer than the bunch replacement time based on polarization loss.

Coherent instabilities in the electron ring have been studied using a modified version of the computer code TRANFT [20], which was used during the design of the National Synchrotron Light Source II (NSLS-II) and evolved into the stochastic cooling simulation code. The code has evolved and now can simulate both single bunch and coupled bunch instabilities, by tracking of up to 5 bunches and assuming a uniform fill. This allows one to use a few times 10^5 simulation particles per bunch when doing coupled bunch calculations.

Simulations were done for 5, 10, and 18 GeV, and the results are summarized in Tables 7 and 8. The code tracks the longitudinal and a single transverse dimension. The four impedance values in Table 8 along with the short range resistive wall and Coherent Synchrotron Radiation (CSR) impedance were included. The beam-beam force was enough to damp transverse coupled bunch modes and a longitudinal damper with a gain of $g_z = 5 * 10^{-3}$ damped the coupled bunch longitudinal oscillations. The damper was applied once per turn and the gain was defined such that

$$\Delta E = - g_z \langle E \rangle$$

where ΔE is the energy kick given to each electron and $\langle E \rangle$ is the average energy error of the electron bunch. It is envisioned that one would use a transverse pickup in a dispersive region with closed orbit subtraction and a filter to notch out the betatron oscillations. The beam-beam parameter was set to 0.1 initially, but values as low as 0.075 were found to be sufficient to stabilize the electrons.

Table 7: Electron Beam Parameters for $|Z/n| = 0.1\Omega$. A uniform fill of 720 bunches was assumed for coupled bunch effects.

Parameter	*5GeV*	*10GeV*	*18GeV*
RF voltage ($h = 7200$) [MV]	20	20	62
RF voltage ($h = 3 * 7200$) [MV]	6.6	6.4	0
γ_T	31	31	41
V_{synch} [MV]	1.3	5.0	38
N_e $[10^{10}]$	31	31	6.3
$\sigma(p)/p$ (Z/n=0) $[10^{-4}]$	8.2	5.5	10
$\sigma(p)/p$ (Z/n=0.1) $[10^{-4}]$	8.6	6.4	10
σ_s (Z/n =0.1) [mm]	22.5	23	8.8

Table 8: Impedances assumed for calculations in Table 7.

Impedance Type	*Rsh*	*Q*	*Fres*
BB longitudinal	51 kΩ	2	20 GHz
BB transverse	1.4 MΩ/m	2	20 GHz
NB longitudinal	360 kΩ	80	856 MHz
NB transverse	10.8 MΩ/m	80	1.0 GHz

After dealing with the coupled bunch modes the main problem was the longitudinal microwave instability which manifested in the classic saw tooth pattern shown in Figure 15. With this impedance and full current we will need to have $\frac{\sigma(p)}{p} = 8.2 * 10^{-4}$. This is within the specifications of the narrow dipoles, but may not be necessary.

In Table 7 the quantity σ(p)/p(Z/n=0.1Ω) is the minimum momentum spread for which the nominal intensity has negligible bunch length oscillations. The bunch length $\sigma_s(\frac{Z}{n} = 0.1\Omega)$ is the corresponding RMS bunch length.

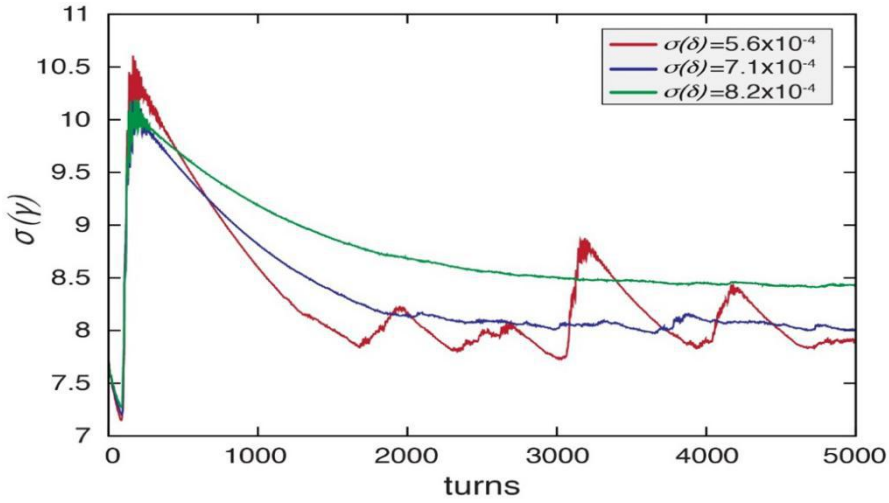

Figure 15: Energy spread in units of rest mass versus turn for 5 GeV electrons with the nominal lattice and various low current σ(p)/p.

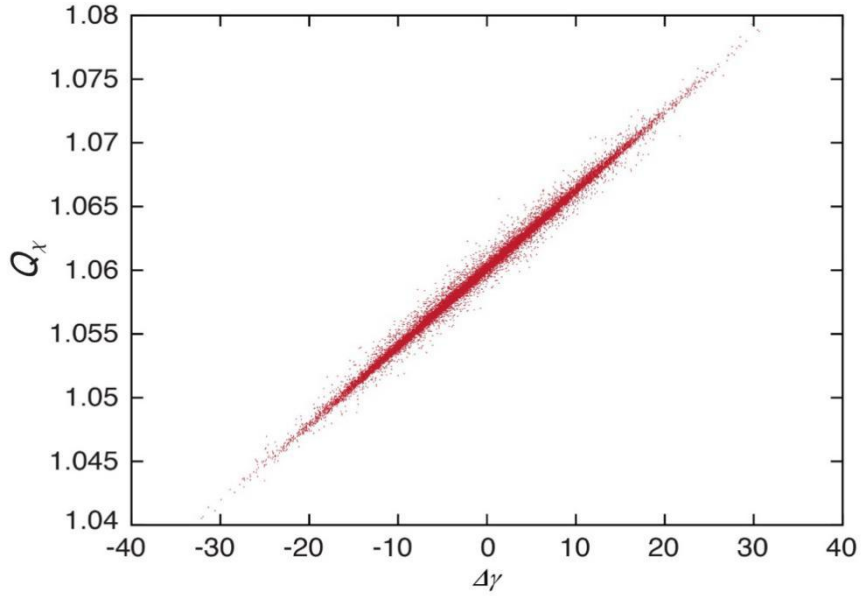

Figure 16: Betatron tune distribution for 5 GeV electrons with an intrinsic momentum spread of σ(p)/p=8.2*10^{-4}.

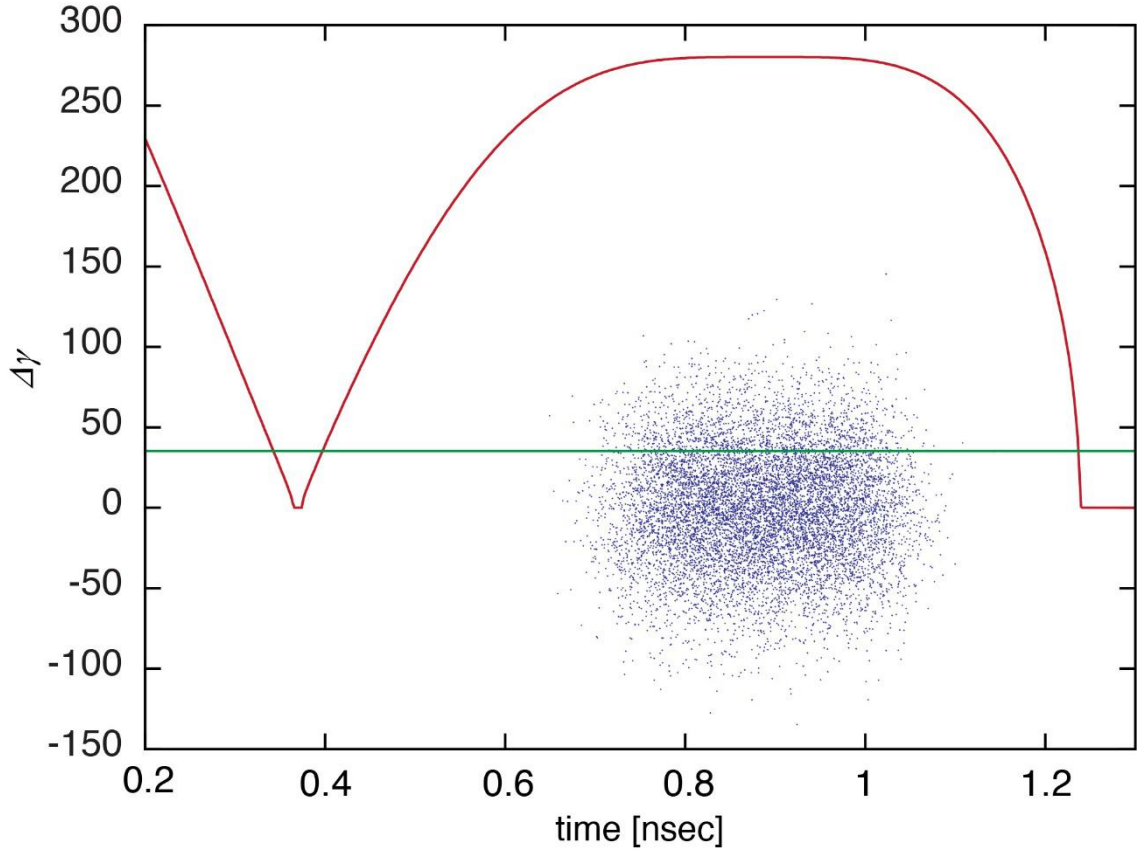

Figure 17: Bunch and bucket for 18 GeV electrons. The horizontal line is at 1.0σ. The full height is 10.5σ

Figure 15 shows the energy spread oscillations for the nominal intensity and various intrinsic momentum spreads at 5 GeV. Figure 16 shows the tune spread for stable beam. Figure 17 shows a nominal 18 GeV bunch within its bucket.

2.2.9 **Hadron Ring**

2.2.9.1 ***Lattice Design***

The present RHIC and its injector complex remain for the most part unchanged when becoming a part of eRHIC. In particular, the arcs with their superconducting magnet structure will remain the same as the present RHIC. Some modifications are necessary or desirable. eRHIC hadrons will circulate in the "Yellow" ring, while the "Blue" ring will remain in place as well. The sextant between IR6 and IR4 of the Blue ring will serve as a transfer line and the beam will be injected in IR4. Some modification of the RF system is necessary to accommodate the 330 bunches at injection and to accomplish the splitting into 1320 bunches. Space for more RF cavities will be provided in IR4 and IR10. The non-colliding straight sections (utility straights) will be simplified by removing the DX separator dipoles in order to simplify the geometry and provide space for the electron ring cross-over from inner to outer arcs and vice-versa.

Studies are underway to investigate whether the D0 magnet can be removed as well. The sextant between IR2 and IR12 of the Blue ring will be used to circulate low energy hadrons which then have the same revolution time as electrons despite their reduced velocity.

2.2.9.2 *Keeping the Hadron Revolution Frequency Constant for all Beam Energies*

Proton and ion beams are not ultra-relativistic in the energy range of an electron-ion collider. In eRHIC, the hadron beam energy is chosen to vary between 41 GeV and 275 GeV. If the beam orbit was the same, the revolution time would vary by 3.3 nsec between these two beam energies. In order to maintain synchronization with the ultra-relativistic electrons, the hadron orbit will be shortened by up to 94 cm for the lowest hadron energy of 41 GeV.

This is accomplished in the following way:

The hadrons circulate counterclockwise in the Yellow ring.

In the arc between IR2 and IR12 the high energy beam (in the 100-275 GeV energy range) travels in the outer arc (a part of the Yellow ring), while the 41 GeV beam passes through the inner arc (a part of the Blue ring).

The inner and outer arc radii differ by 88 cm, and an inner sextant is 94.2 cm shorter than an outer one. This path length difference allows for synchronizing 41 GeV hadron beams with the electrons. When synchronizing higher energies, using the outer arc between IR2 and IR12, the central orbit, passing through quadrupole magnet centers, is used for a proton beam of 133 GeV. For the beam energies 275 GeV and 100 GeV the synchronization can be accomplished by +14 mm and -14 mm radial shifts, correspondingly, which is well within the acceptance of the 80 millimeter diameter vacuum chamber.

The corresponding modifications to the RHIC lattice are only relatively minor. This requires some rearrangement of the bus system. The Blue ring sextants used for injection and low energy running must be powered with reversed polarity. The superconducting magnets of RHIC are protected by cold diodes which in principle must be reversed. However, quench analysis shows that at less than 20% of maximum excitation, this protection is not required.

Thus, modifications of the RHIC lattice and magnet system for eRHIC are fully reversible and are accomplished with relatively little effort.

2.2.9.3 *Hadron Ring Dynamic Aperture*

The strong focusing of the hadrons at the collision point causes maximum β-functions in the low-β quadrupoles to exceed $\beta_x = 1600\,m$ and $\beta_y = 1300\,m$. The contribution to the natural chromaticity generated in one IR amounts to $\xi_x = -30$ and $\xi_y = -40$, which is 20% of the contributions from the 90 degree arcs. This implies a large contribution of the chromaticity generated in the interaction region that must be compensated by sextupoles in the arcs in order to confine the tune footprint of the hadron beam to remain within the space between nonlinear resonance lines.

As discussed above, the strength of these resonances is enhanced by the nonlinear field, and the resonance free space in the tune diagram is shrinking. Obviously, there is a maximum amount of IR chromaticity and corresponding tune footprint which can be accepted. This chromaticity limit is determined by numerical particle tracking to verify that the dynamic aperture is sufficiently large. The numerical simulations also include the impact of field errors of the superconducting magnets, the magnets in the interaction regions, and imperfections such as magnet misalignment.

The dynamic aperture is defined as the maximum betatron amplitude within which particles are not lost in a given number of turns of single particle tracking. The long-term dynamic aperture converges to the boundary between regular and chaotic motion. Experience with RHIC operations indicates that relevant dynamic aperture figures require tracking over 10^6 turns. The stability of a particle is assessed by the analysis of the trajectories over 10^6 turns which allows one to characterize a trajectory as stable or unstable.

The results of such simulations show that the dynamic aperture of the eRHIC hadron ringm amounts to 10σ at injection and 6σ at high luminosity operation. The simulation includes the beam-beam effect in weak-strong approximation. This is the same value as obtained for present RHIC.

2.2.9.4 *Electron Cloud Effects*

Electron clouds are a serious concern for the ion ring with 1320 bunches and $0.6 * 10^{11}$ particles per bunch. Electrons which are produced in the beam vacuum chamber by ionization of the residual gas by the beam may get accelerated by the following bunches and may hit the vacuum chamber wall with high energy, thereby releasing more electrons from the wall. This mechanism may create an electron avalanche that builds up rapidly as the entire bunch train passes by. The consequence could be high cryogenic losses and beam instabilities. Next to beam current and bunch parameters,

the key parameter that determines the seriousness of the electron cloud effect is the secondary emission yield (SEY, number of emitted electrons from the surface per incident electron) coefficient of the vacuum chamber material.

We assume that the stainless steel beam pipe of RHIC will be coated with copper and that we will be able to improve the secondary emission coefficient by scrubbing the surface by beam operation to the level achieved in the LHC [21].

An initial simulation using the computer code CSEC [22] and a model for the wall parameters in the scrubbed LHC showed dangerous electron clouds both for the LHC and for eRHIC, with LHC being slightly worse. For both machines the average dose to the wall was in the tens of watts per meter range but this value depends critically on the assumed secondary emission yield, which was inferred for the LHC using the measured energy deposition.

eRHIC requires a stronger suppression of the electron cloud mechanism in order to keep the cryogenic load within tolerable limits of $P_{load} \leq \frac{1W}{m}$. This is planned to be achieved by an additional layer of coating consisting of amorphous carbon. For electron clouds we are collaborating with CERN in understanding and reproducing their results. In the end we know that electron clouds in the LHC are difficult but tractable. There is currently no reason to believe otherwise for eRHIC.

2.2.9.5 *Intra-Beam Scattering*

The effect of multiple Coulomb scattering of charged particles inside a bunched beam upon each other taking into account the Lorentz boost is known as Intra-Beam Scattering (IBS) [23] This causes emittance growth in all oscillation planes of the beam. This effect limits the high beam density needed for high luminosities, and it affects the luminosity lifetime and the average luminosity. Beam parameters thus must be chosen to achieve an IBS growth time of several hours given the beam set-up time of typically 1 hour, unless the emittance growth can be overcome by strong active cooling of the beam emittances. Table 9 lists the beam parameters and calculated IBS growth times for the eRHIC design parameters of protons at 41 GeV, 100 GeV, and 275 GeV.

Table 9: eRHIC Proton Beam Parameters.

Parameter	***Moderate luminosity without cooling***			***High luminosity with cooling***		
Beam energy [GeV]	41	100	275	41	100	275
Bunch intensity [10^{11}]	0.6	1.1	1.1	0.11	0.6	0.6
RMS Horizontal normalized emittance [mmmrad]	3.3	4.5	4.1	2.0	3.6	2.7
RMS Vertical normalized emittance [mmmrad]	2.5	2.5	2.5	0.11	0.19	0.4
Longitudinal bunch area [eVsec]	0.5	0.6	0.8	0.2	0.4	0.4
RF frequency [MHz]	225	225	563	563	563	563
RF voltage [MV]	8	11	24	8	16	18
RMS momentum spread [10^{-4}]	15	8.7	6.6	10.3	9.1	4.6
RMS bunch length [cm]	13	11	7	7.5	7	5
Longitudinal Emittance IBS growth time [hours]	10.3	8.	10.1	3.2	2.4	2.2
Horizontal Emittance IBS growth time [hours] (without coupling)	8.0	13.7	9.2	2 0	2.0	2.1

For the high luminosity parameters as listed in Table 9, beam growth due to IBS is significant and strong cooling is required to maintain the beam density and the luminosity over a reasonable store time of at least several hours. These parameters are based on new 225 MHz and 563 MHz RF systems for the hadron ring that would have to be added to the present RHIC. The results are based on complete decoupling of horizontal and vertical betatron motion. This is also essential to maintain unequal emittances in the horizontal and vertical plane. Very good vertical orbit control is also mandatory to avoid any significant vertical dispersion. With strongly suppressed vertical dispersion there will be no significant emittance growth due to IBS in the vertical plane.

2.2.9.6 *Hadron Ring Strong Beam Cooling*

Highest luminosity in an electron-ion collider can only be achieved by introducing a strong beam cooling mechanism that counteracts IBS, which would otherwise cause rapid increase of emittance and reduction of luminosity. Moreover, the hadrons which gained large transverse and longitudinal amplitudes by IBS experience a strong nonlinear force due to the beam-beam force imposed by the electron beam that would enhance halo formation and experimental backgrounds. Thus, with the parameters required for high luminosity, the hadron beam would become unusable quickly without cooling and would have to be replaced frequently.

As the turnaround time of superconducting RHIC is about 1 h, based on slow magnetic cycle of RHIC main magnets and spin rotators and the filling time at injection, the increase of peak luminosity above a certain level of performance would lead to a reduction of average luminosity. The eRHIC High Luminosity parameters (see parameter Tables 1 and 9) were selected to have an IBS growth time $\varepsilon/(d\varepsilon/dt)$ of no less than two hours in order to ease requirements on the hadron cooler.

Stochastic cooling is a well-established cooling mechanism for hadrons which has been pioneered at RHIC for bunched ion beams. It is used very successfully for cooling of gold beams in RHIC operations and has enhanced the luminosity significantly. It would work in principle for protons at high energies, but the cooling rates at typical intensities of eRHIC proton bunches fall short of the need by *orders* of magnitude because of bandwidth limitations of beam pick-up and kicker magnets.

Electron cooling with a DC electron beam is a standard cooling mechanism for hadron beams that works well at low hadron energies up to a few GeV. For large hadron energies of multi-GeV, however, this cooling method becomes quite unfeasible as the cooling time scales strongly with the beam energy as $\gamma^{5/2}$, with γ being the relativistic factor of the hadrons. Furthermore, the electrons have to have the same relativistic factor as the hadrons and DC electron energies of tens of MeV are not available.

Using bunched electron beams accelerated by an RF LINAC would mitigate this somewhat. However, the cooling of 275 GeV hadron beams is still extremely challenging with incoherent electron cooling and the effort in cooling installation becomes unrealistically large because of large required electron beam currents on the order of amperes.

We are also looking into more recent approaches for strong hadron cooling. A novel method of hadron cooling which promises to work at very high hadron beam energies has been proposed [7]. This method, which is called "coherent electron cooling", uses an electron beam to pick up the longitudinal Schottky noise of the hadron beam, and subsequently amplifies the signal by sending the electron beam through a free electron laser. The strongly micro-bunched electron beam is then merged with the hadron beam with proper timing. The electron beam then acts as a kicker to reduce the energy spread of the hadron beam.

Recently, a variant of this method has been proposed [24] which achieves the micro-bunching by sending the beam through a chicane or a series of chicanes with optimized R_{56}. This method has limited amplification of the signal but reaches extremely large bandwidth.

A proof-of-principle experiment on a low energy RHIC ion beam is underway that aims at demonstrating coherent electron cooling with FEL amplification. This experiment is expected to provide results in 2018 [1].

Figure 18 shows a sketch with the layout of the proposed coherent electron cooling system for eRHIC which is laid out to support the storage of hadron beams required for luminosities in the range of $10^{34}\mathrm{cm}^{-2}\mathrm{sec}^{-1}$. An electron beam generated by a superconducting RF gun is injected into a three-turn energy-recovery superconducting LINAC that provides an energy gain of 50 MeV per passage. The fully accelerated electron beam of up to 150 MeV is injected onto an orbit which overlaps with the orbit of the eRHIC hadron beam in the straight section of IR10 over a distance of 50 m, which is called the modulator section. After this first common section, the hadron beam propagates through a section with an appropriately tuned $R_{56} = \lambda_{FEL}/(\Delta p/p)_{RMS}$ which separates particles with positive and negative energy deviation by a longitudinal distance corresponding to the width of the micro-bunch peak of the electron beam.

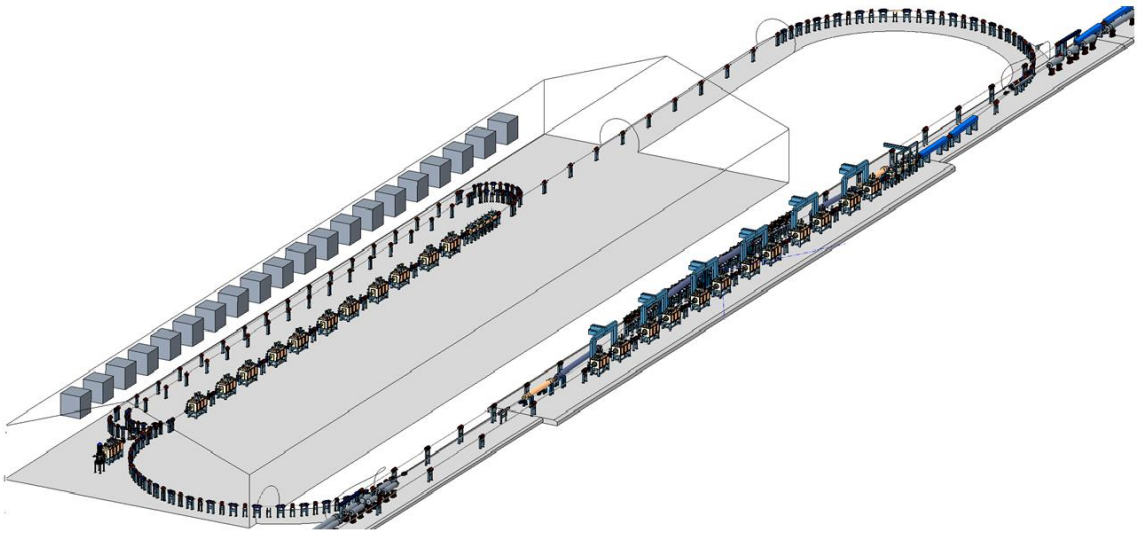

Figure 18: Rendering of the proposed layout for coherent electron cooling at eRHIC

The electron beam is energy-modulated due to residual fluctuating space charge forces from the proton beam. The electron beam passes through a chicane where the energy spread caused by the hadron beam density fluctuation is transformed into a micro bunching of the electron beam. The density modulation of the electron beam is then amplified by a mechanism exploiting plasma oscillations:

After one quarter plasma oscillation wavelength, the density modulation is transformed into a now even larger energy modulation, which after a second chicane is turned into a stronger density modulation.

The present stage of the development proposes two amplification stages to produce a sufficiently strong electron density modulation. The electron beam is again launched onto the hadron orbit thereby overlapping with the hadron beam with carefully adjusted phase.

Hadrons with higher energy will be ahead of the electron micro-bunch and will be decelerated. Hadrons with lower energy will trail behind the electron micro-bunch and will be accelerated. The energy spread of the hadrons will be reduced after this `kicker' section. Cooling times of 100 min are envisioned. Table 10 summarizes the parameters of eRHIC coherent cooling.

Table 10: Parameters of the eRHIC coherent electron cooling.

Parameter	***Value***
Hadron Energy Range [GeV]	41-275
Electron Beam Energy [MeV]	22-150
Electron Beam Current [mA]	100
Electron Peak Current [A]	10
Electron Charge per bunch [nC]	0.75
Primary R_{56} [m]	3×0.04
Plasma Amplification stages	2
Secondary R_{56} [m]	0.05
Length of the modulator section [m]	50
Length of the kicker section [m]	50
Cooling Time [hour]	.5

2.2.10 **Electron Injection Complex**

2.2.10.1 ***General Considerations***

The requirements on the electron injector complex are driven by the need for polarized electrons in electron-ion collisions. The electron polarization should be close to 80%. It is also necessary to have two electron spin polarization directions simultaneously present in the same store. This is important to discriminate against systematic errors in the detection. We already discussed the consequences for the injection system but summarize here the chain of arguments:

In principle, electron polarization in a storage ring builds up by the so-called Sokolov-Ternov effect: Spin flips are induced in the process of emitting synchrotron light photons.

Spin flips from spin which is parallel to the magnetic dipole field to spin which is antiparallel when emitting photons are slightly more likely than the opposite spin flip. The differential flip rate leads to a slow build-up of polarization antiparallel to the magnetic dipole field. Unfortunately, the polarization build-up time is much too slow to be of practical use at eRHIC electron energies. Consequently, the spin polarization for eRHIC electron beams must be produced at the source and must be preserved during the acceleration process.

The bunches which are polarized parallel to the magnetic guide field are subject to slow depolarization by the Sokolov-Ternov effect in the storage ring. At 18 GeV operation, a bunch replacement rate of once per 6 *min* for each individual bunch in the storage ring is required to keep the time-averaged level of polarization larger than approximately 84% of the injected polarization. Thus the injector has to provide a new bunch about every second to maintain good polarization of all 330 bunches. At 10 GeV and 5 GeV, the depolarization time is much longer, and the bunch replacement rate can be reduced by a factor of at least five.

The injector will deliver electron bunches which are 85% spin polarized at beam energies of 5 GeV, 10 GeV, and 18 GeV. In the storage ring the highest bunch charge of 50 nC is required for operation at 10 GeV and 5 GeV without hadron cooling whereas for 18 GeV operation a bunch charge of 10 nC is more than sufficient. In order to reach the storage ring bunch intensity of 50 nC at 10 GeV five bunches from the injector need to be accumulated in one storage ring bucket. Thus the injector has to deliver 10 nC at a 1 Hz rate. These bunch charge and rate requirements are sufficient for operation at all energies with and without hadron cooling, as shown in Table 11.

The electron injection complex consists of the following elements:

- Electron gun with a Ga-As photo-cathode;}
- Low energy transfer line (0.4 *MeV*);
- Electron S-band LINAC (400 *MeV*);
- Medium energy transfer line (400 *MeV*);
- Rapid cycling electron synchrotron (0.4-18 *GeV*) in the RHIC tunnel;
- High energy transfer line (5-18 *GeV*).

Table 11: Requirements for the electron injector.

Parameter	*Moderate luminosity without cooling*			*High luminosity with cooling*		
Energy E [GeV]	5	10	18	5	10	18
Ext. E_k from Source ($\gamma = 1.27$) [keV]		350			350	
LINAC energy gain [MeV]		400			400	
Normalized electron emittance after LINAC [μm]	125	95	115	20	20	115
Beam emittance at RCS extraction [x/y, nm]	20/13	20/4.9	22/3.3	20/2	20/1	22/3.3
Bunch Charge in Storage Ring [nC]	50	50	10	25	25	10
Number of Bunches in Storage Ring	660	660	330	1320	1320	330
Bunch Charge in Source and RCS [nC]	10	10	10	5	5	10
Ramp Rate [Hz]		1			1	
Bunch Replacement Period [min]	55	55	5.5	110	110	5.5
Bunch replacement period (polar. req.) [min]	149	118	6.6	149	118	6.2

2.2.10.2 *Polarized Electron Source*

The requirement for the polarized eRHIC source is a charge of 3-10 nC of 85% polarized electrons at a rate of 1 Hz and a normalized transverse emittance of 10-30 μm This requirement satisfies the needs for all operation modes of the storage ring.

Polarized electron beams are obtained from special photo-cathodes. The most common material which has been used successfully in the last 30 years is Ga-As alloy. Strained Ga-As cathodes which are irradiated with UV laser light of 780 nm yield high polarization of the extracted electron beam and a high quantum efficiency (QE $\geq$ 1%) when coated with a mono-layer of Cs.

The polarized electron gun of the Stanford Linear Collider (SLC) which was developed in the 1980's provided a reliable performance delivering 16 nC of polarized electrons (70-75% polarization) at 120 Hz repetition rate. In principle, the eRHIC injector could be based on the SLC gun. However, to exploit the technical development which has occurred in the last three decades, a dedicated eRHIC gun has been designed which promises larger beam energy, longer cathode lifetime, higher reliability, and larger polarization ($\geq$ 80%). A comparison of gun parameters is shown in Table 12.

Table 12: Electron source parameters.

Project	*RF Frequency [GHz]*	σ_s *[ps]*	*Bunch Charge [nC]*	*Energy [MeV]*	*Emittance [μm]*	$\Delta\gamma/\gamma$ [%]	*Cathode Material*
SLC 5mJ,845nm Laser	DC	2000	$9-16$	0.12	15	1.5	Ga-As
eRHIC 5mJ,780nm Laser	DC	2000	$3-10$	0.35	$10-30$	2	Ga-As super lattice

A new gun geometry based on the "inverted gun"-scheme has been designed. The design is optimized for a high extraction voltage of 350 keV and low electron beam loss. For good cathode lifetime and high reliability, excellent vacuum conditions are needed in the gun, the extraction line, and the tune-up beam dump. A prototype of this beam line has been built and tested. A load lock system for installation of prepared and activated cathodes into the gun has been designed. A prototype of this system is available and has been tested.

2.2.10.3 *Rapid Cycling Synchroton*

Full energy injection of polarized electron bunches is accomplished by a Rapid Cycling Synchrotron (RCS) in the RHIC tunnel which accelerates the electrons from the 400 MeV LINAC to up to 18 GeV for injection into the storage ring. The synchrotron has a repetition rate of 1 Hz and a total ramping time of 200 msec. The most important design feature of the synchrotron is spin transparency up to the full energy of 18 GeV. This is accomplished by high lattice periodicity P. The RHIC tunnel, however, only allows a lattice symmetry of 6 as it is composed of 6 arcs separated by 6 straight sections. This design overcomes this limitation by configuring the straight section beam optics such that the transformation of beam coordinates through the straight section is an identity transformation. This also includes the electron spin. In order to suppress intrinsic depolarizing resonances, the periodicity P and the vertical betatron tune $Q_{y,\,arc}$,

calculated by accounting betatron phase advance in the arcs only, must fulfill the conditions:

$$P - Q_{y,\,arc} > a\gamma$$

And

$$Q_{y,arc} > a\gamma \qquad (6)$$

where $a\gamma = 40.849$ is the spin tune with $a = 1.16 * 10^{-3}$ being the anomalous magnetic moment of the electrons. This leads to the choice of $Q_{y,\,arc}$~50 and P = 96 which is readily accomplished given the large arcs of RHIC. The lattice in the arcs is thus composed of $6 * 32$ FODO cells with a betatron phase advance of π/2. A super-period consists of two FODO cells as there are two sextupole families per plane to compensate linear and nonlinear chromaticity. A special feature of one of the straight sections is that the synchrotron orbit must pass around the colliding beam detector with a spin transparent chicane.

At the peak energy of 18 GeV, the electrons suffer from an energy loss of 36 MeV/turn due to synchrotron radiation. The acceleration and radiation loss compensation is done by 13 eight-cell 563 MHz RF cavities powered by IOT amplifiers.

The synchrotron accelerates single bunches with a charge of 10 nC. With this amount of bunch charge, the electron beam remains below any collective instability threshold. A third harmonic system is being studied which could provide additional stability margin.

The concept of spin transparent acceleration was tested extensively by comprehensive simulation studies. The amount of depolarization during the acceleration was found to be only in the order of two percent. These simulations take into account an imperfect machine lattice. In order to obtain realistic estimates on the preservation of electron spin polarization, imperfections of quadrupole fields, typical betatron coupling, misalignment and closed orbit errors as well as sextupole fields for chromaticity corrections have been introduced in the machine model.

Correction algorithms have been applied to adjust correction elements such as dipole correctors, tune correction quadrupoles and skew quadrupoles. It is assumed that orbit excursions can be kept below 0.5 mm. It is further assumed that the betatron tunes during the ramp are kept within $|\Delta Q| \leq 0.01$ by applying tune feedback or pre-programmed time-dependent tune corrections.

With this realistic machine model, simulations show that the polarization is robust and resilient against residual imperfections (see Figure 19). These good polarization results are consistently obtained for a number of statistical error seeds.

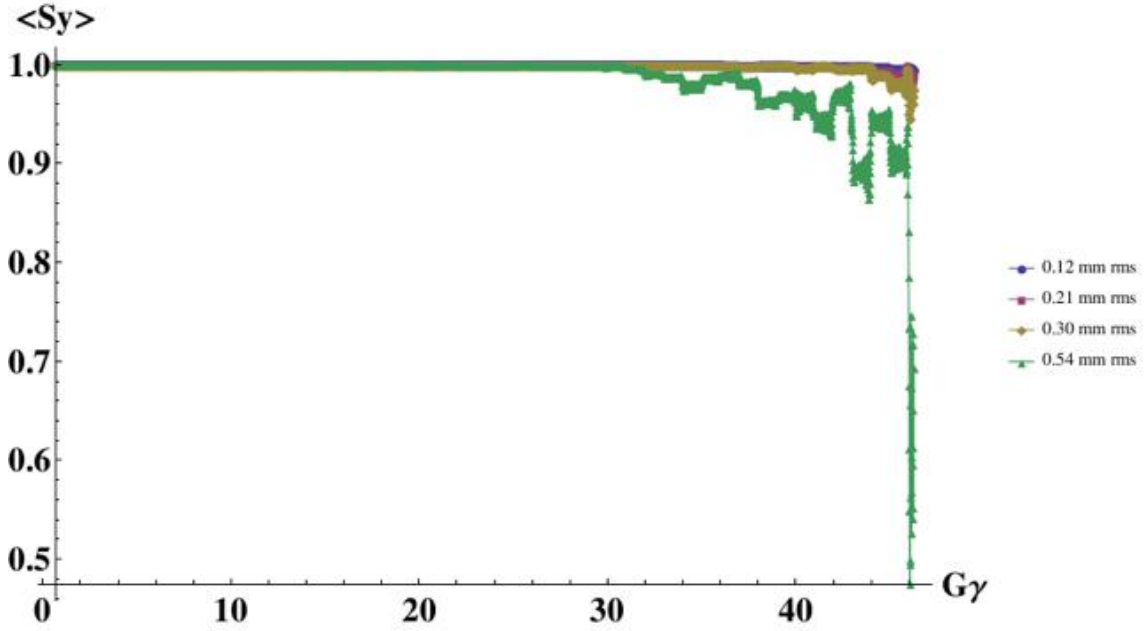

Figure 19: Electron spin polarization in the Rapid Cycling Synchrotron as a function of beam energy expressed in terms of spin tune $a\gamma$ during the ramp. Different color curves indicate different RMS values of residual orbit distortions. Note the suppressed zero of the vertical scale

2.2.10.4 *Electron Injection*

The requirement of arbitrary spin patterns in the electron ring coupled with radiative polarization necessitates regular bunch replacement. At an electron beam energy of 18 GeV, we plan to replace electron bunches every 6 min. With 330 bunches this corresponds to 1 sec between injections. The electron injection is accomplished by a combination of fast and slow kickers and a pulsed eddy current injection septum in the horizontal plane. The slow kickers form two closed three-bumps. The first one is used to extract a bunch with depleted polarization to create an empty bucket for the fresh bunch. It kicks a large fraction of the stored beam to transverse amplitudes close to the extraction septum. A fast kicker magnet right next to the first slow bump kicker kicks only the bunch that will be extracted and is going to be replaced by a fresh, injected bunch. The additional kick allows the selected bunch to enter the extraction septum.

The second slow bump is for injection. The storage ring beam optics has a dispersion at the injection septum where the second slow bump has its maximum spatial excursion. The new bunch is extracted from the RCS with a slight energy offset with respect to the energy of the circulating beam in the storage ring. The energy offset times the dispersion equals the distance of the bunch to be injected from the orbit of the circulating beam. This scheme results in injection without a transverse oscillation amplitude, but with a longitudinal oscillation amplitude. The offset of the injected beam with respect to the closed orbit vanishes at locations where the dispersion is zero which is in particular the case in the IR. The longitudinal injection oscillation will be eventually removed by radiation damping. The scheme is illustrated in Figure 20.

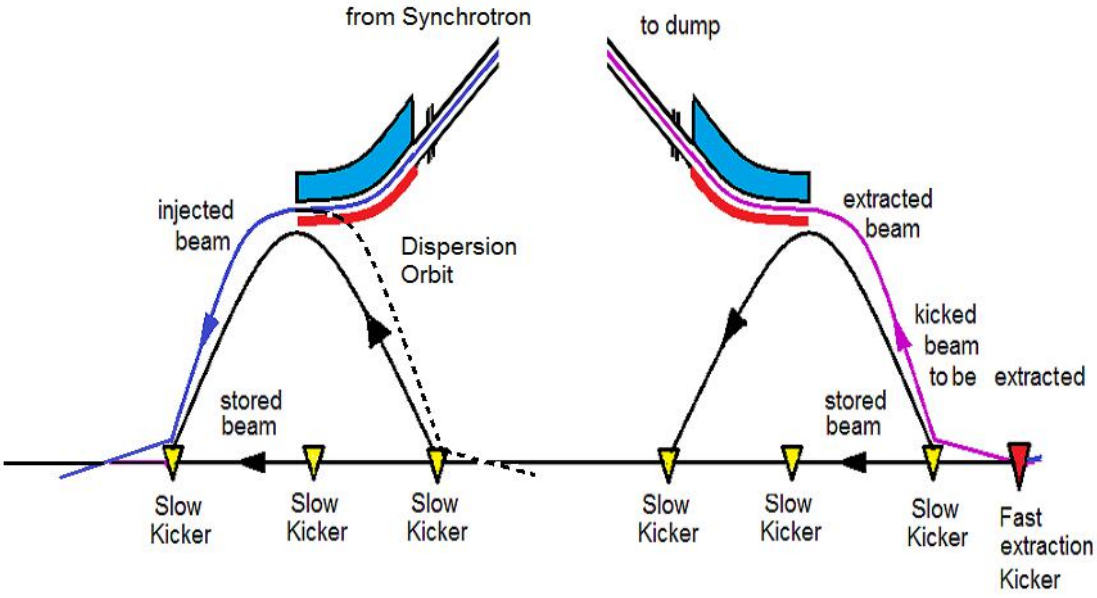

Figure 20: Electron injection and extraction scheme, based on two slow 180 degree kicker bumps, one for extraction (right hand side) and one for injection (left hand side) which bring the stored beam within three horizontal RMS beam sizes ($\sigma_x = \sqrt{(\varepsilon_x \beta_x + D_x^2 \sigma_E^2)}$ to the injection and extraction septum, respectively. The bumps rise in $13\mu sec$ (one turn around the accelerator) and return to zero during the following 13μsec. The dispersion at the injection septum is non-zero. The beam to be injected has a slightly different energy than the stored beam and the distance between the center of the stored beam and the beam to be injected equals the dispersion times the relative energy difference between stored and injected beam. This way the beam is injected in the center of horizontal phase space but off-center in the longitudinal phase space. For extraction, a fast kick is required on top of the slow bump to kick the beam into the extraction septum

2.2.11 **Hardware Systems of the eRHIC EIC**

By far the largest fraction of present day RHIC will remain unchanged for eRHIC. There are only very few technical components of the hadron storage ring which need some upgrade for eRHIC operation. These will be discussed in the following sections.

2.2.11.1 ***Hadron RF Systems***

The largest modification concerns the RF system. The hadron bunches from AGS with a bucket area of $1.6\text{eV} * \text{sec}$ will be received by the existing 28 MHz RF system which will also be used to accelerate the beam to full energy. The existing 197 MHz system is no longer needed. For maximum luminosity operation, each hadron bunch will be adiabatically split into four bunches by a two-stage beam splitting scheme. This requires two new 112.6 MHz RF cavities.

The split bunches need to be pre-compressed by a 225 MHz RF system (4 cavities) before they can be accepted in a storage cavity system with 563 MHz. These cavities will be superconducting and are identical to the electron storage ring cavities. Three 2-cell cavities will be required to squeeze the bunches to 7 cm bunch length, which requires 8 MV of RF voltage per cavity.

2.2.11.2 *Hadron Injection Kicker*

Another modification that is required is a new kicker system that is re-designed for a shorter rise time. The 28 MHz bunch frequency (bunch spacing $T_s = 35.5\,\mathrm{nsec}$) is three times larger than the present RHIC bunch frequency which requires new, faster injection kickers. The new kickers have a rise time which is three times shorter than the present injection kicker system, less than 12 nsec. The 20 kicker units have a total length of $\cong 25\,\mathrm{m}$. The new injection kickers will be placed in the straight section of IR4. The corresponding updates of the magnetic elements in IR4 are only minor.

2.2.11.3 *Hadron Collimation*

The present RHIC collimation system needs to be improved for the needs of an electron-ion collider. A two-stage system with optimized phase advance between the primary and secondary collimators like in HERA is planned. In addition, a system with non-zero dispersion for momentum collimations is foreseen. The hadron collimation system is planned to be installed in IR12.

2.2.11.4 *Copper Coating of the RHIC Beam Pipe for Hadrons*

The high peak current of the eRHIC proton beam ($\cong 200$ mA) with its large number of short, high intensity bunches results in unacceptably high heat load of the cold stainless steel beam pipes in the superconducting RHIC magnets. To reduce this heat load to levels below 1W/m, which can be compensated by the RHIC cryogenic system, the conductivity of the beam pipe has to be increased. This will be accomplished by in-situ copper coating of the entire RHIC ring.

To prevent electron cloud build-up due to the short bunch spacing the secondary electron yield (SEY) of the beam pipe surface has to be reduced below 1.2. Thorough "scrubbing" of the newly applied copper coating using a plasma discharge cleaning technique might accomplish that, but in order to reduce risk, it is also planned to apply a layer of amorphous carbon to safely reduce the SEY below the critical value.

2.2.11.5 *Electron Storage Ring Magnets*

The magnet system of the electron storage ring consists of conventional iron-dominated room temperature electro-magnets. They have hollow, water cooled conductors. The current density is below $5\mathrm{A/mm}^2$ and the magnetization of the yoke does not exceed 1.4 T. High quality magnetic steel (AISI 1006) is assumed. It is not decided at this point whether to machine yokes from solid blocks or build the yokes from fine blanked laminations.

The bending magnets in the regular FODO structure are split into three magnets, two 2.66 m long ones with field strength of up to 0.248 T and a short magnet in-between which is 0.45 m long with a maximum strength of 0.7 T. There are 252 of such triplets. Figure 21 shows a rendering of these magnets.

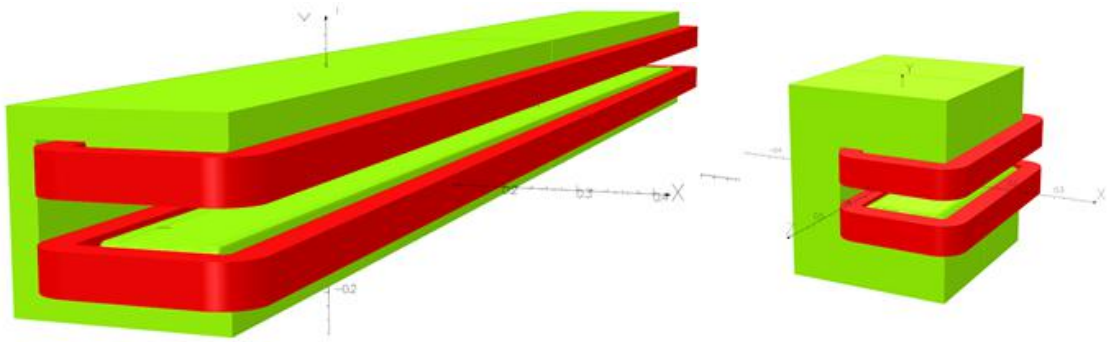

Figure 21: Short and long units of the dipole magnet triplet of the electron storage ring

The field quality of the dipoles is controlled by chamfering of the yokes which reduces the largest field harmonic (sextupole) to -1.4 units of 10^{-4} relative field error at 25 mm. This is subject to further optimization.

There are 494 conventional quadrupole magnets with a maximum field gradient of 18.4 T/m. The quadrupole magnet is 0.6 m long and its outer dimensions are 0.42 m*0.42 m. The cross section of the quadrupole is shown in Figure 22 and the cross section of the sextupole magnet is shown in Figure 23.

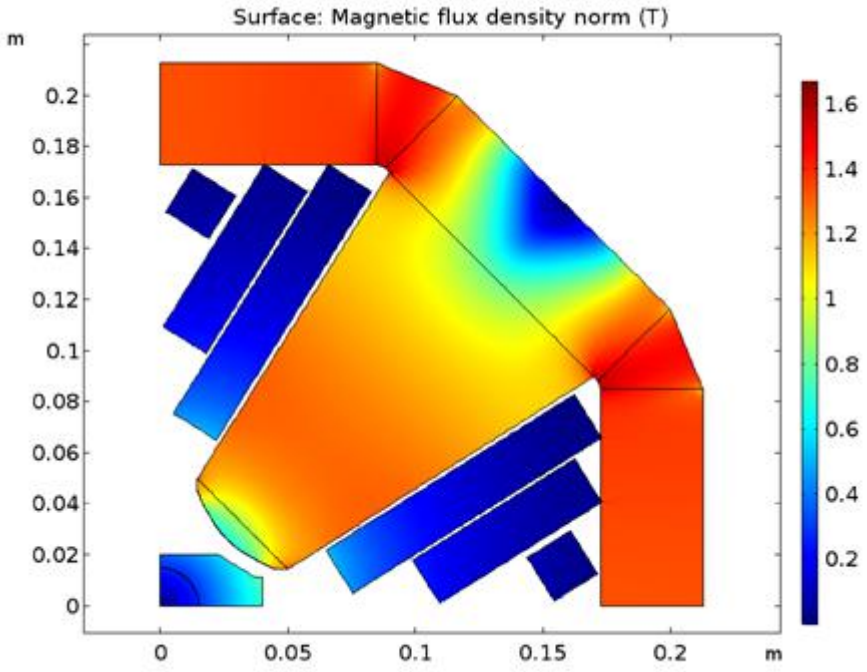

Figure 22: Cross sections of the quadrupole magnet; the color code indicates the field strength in tesla. The largest harmonic is a 12-pole component of $1.8 * 10^{-4}$ at 25 mm referring to the integrated gradient field at 25 mm which is 0.276 Tm.

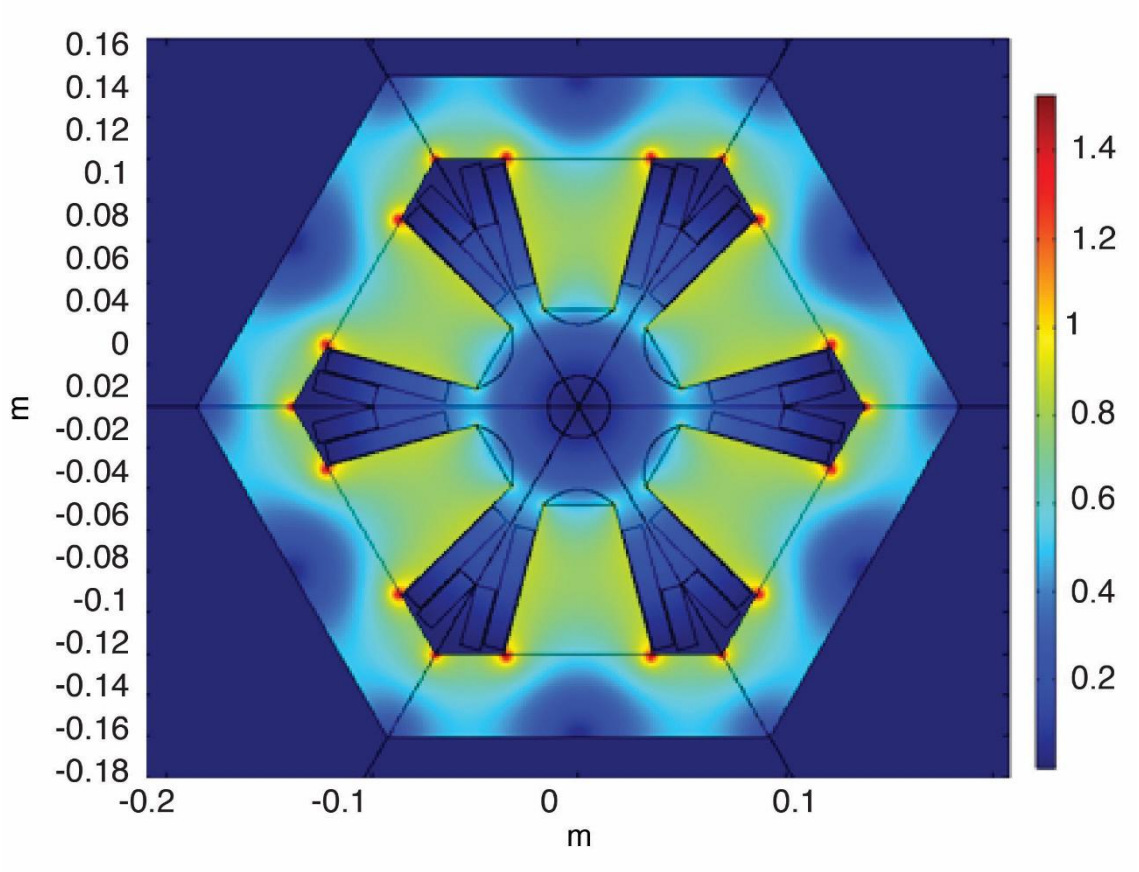

Figure 23: Cross section of the sextupole magnet; the color code indicates the field strength in tesla.

The total power consumption at the highest beam energy of 18 GeV is 3.3 MW. Figure 24 depicts the power consumption for each type of magnet versus the electron beam energy.

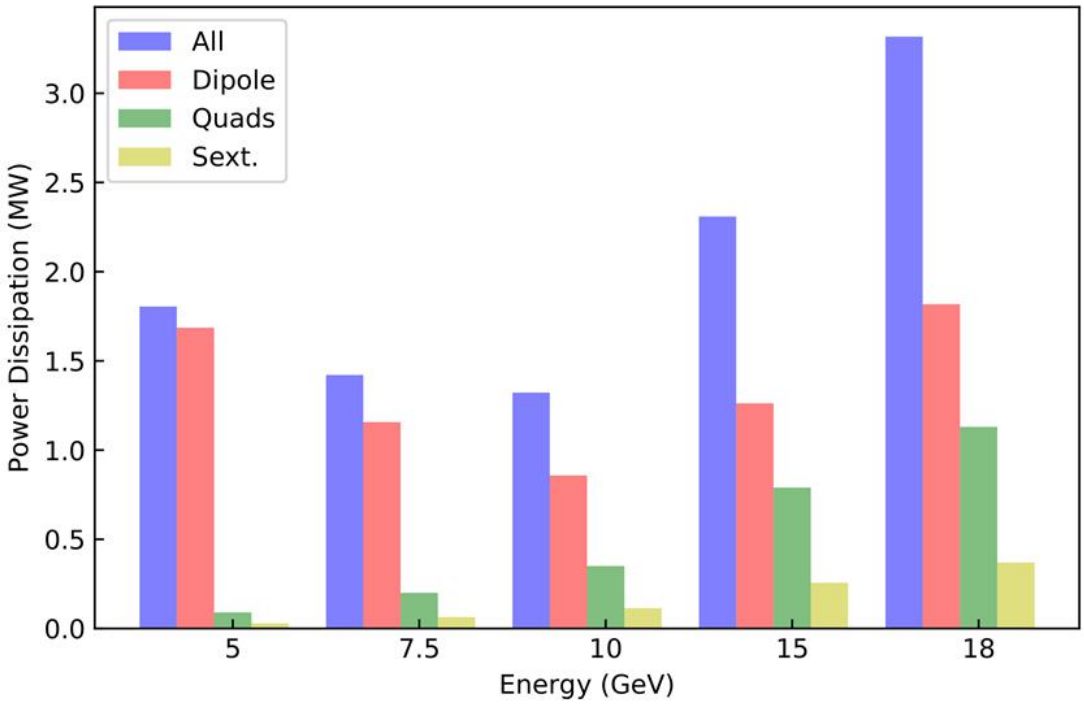

Figure 24: Power dissipation of storage ring magnets for operation energies 5 GeV to 18 GeV.

2.2.11.6 *Vacuum System of the Electron Storage Ring*

The eRHIC Storage Ring vacuum system consists of 3.8 km of vacuum chamber separated into 36 vacuum sections. Each of the arc vacuum sections is comprised of eight arc FODO cells. Each FODO cell has two 6.2 m long dipoles which are split in three parts each with a common vacuum chamber and two 1.7 m long quadrupole chambers. The quadrupole chambers accommodate the quadrupole, sextupole and corrector magnets, the beam position monitors, synchrotron radiation masks, and pump ports. The chambers are separated by RF shielded bellows.

There are also twelve vacuum sections for the 1.2 km of straight section and in addition twelve sections with specialized equipment such as interaction region, RF-sections, and beam injection/extraction. The sections are separated by gate-valves which allow one to isolate the vacuum sections from each other. The vacuum chambers are pumped by NEG-strips, NEG cartridges, titanium sublimation pumps and ion getter pumps. The vacuum system is designed for a pressure of 10 nTorr with full beam current of 2.7 *A*. The lifetime due to bremsstrahlung from scattering off the rest gas is larger than 20 hours for all beam energies from 5 to 18 GeV.

The thermal load from synchrotron radiation hitting the beam pipe is considerable. A total synchrotron radiation power of up to 10 MW is accommodated by the water cooled vacuum chamber. On average, the vacuum chamber is exposed to a linear power density of 6 kW/m if the beam energy is between 10 and 18 GeV. With the horizontal aperture of 80 mm, the emitted synchrotron radiation travels on average 5 m before it hits the vacuum chamber. With a horizontal beam emittance of ε=24 nm and an emittance ratio of $\kappa = \frac{\varepsilon_y}{\varepsilon_x} = 0.02$, the synchrotron radiation spot of the 18 GeV beam has

a beam height of 128 μm when it hits the vacuum chamber. This corresponds to an average power density of $37\frac{\mathrm{W}}{\mathrm{mm}^2}$.

A material with good heat conductivity properties has to be chosen which has at the same time good vacuum properties, good mechanical stability and will allow standard manufacturing processes such as extrusion, welding or brazing. Such a material is the Cu-Cr-Zr alloy which has a heat conductance close to that of copper and excellent manufacturability. In addition this material has excellent yield strength and is less costly than materials with comparable properties. Figure 25 shows a cross section of the vacuum chamber.

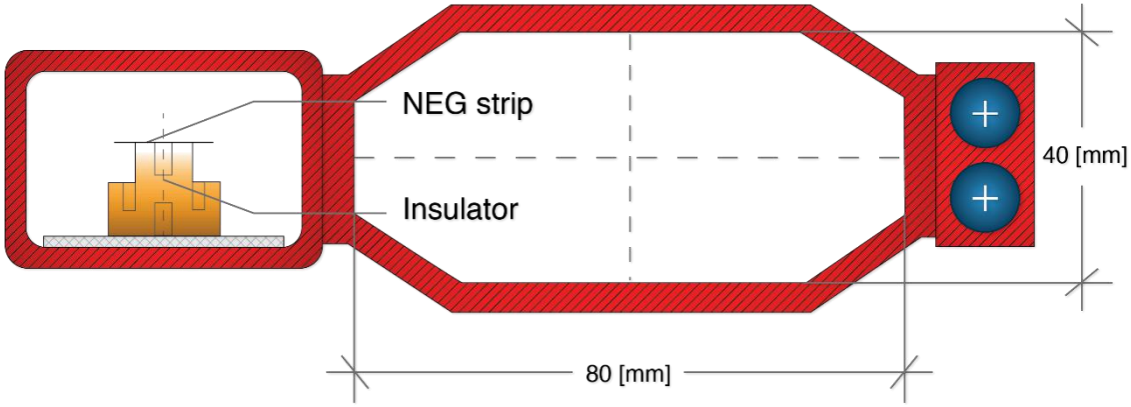

Figure 25: Cross section of storage ring vacuum chamber in dipole magnets

With a cooling water velocity of 2 m/sec, the maximum temperature on the inner surface of the dipole chamber is about 100^{o}C. Figure 26 shows the temperature distribution on the dipole chamber inner surface.

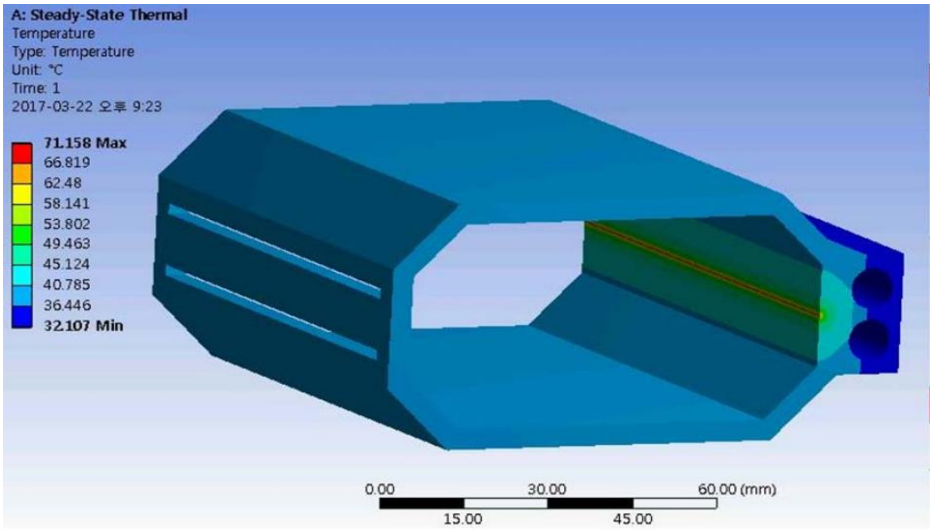

Figure 26: Analysis of the temperature distribution of the dipole chamber which is exposed to the full synchrotron radiation power

The chamber can be fabricated by extrusion. The pumping screen, flanges, and pump port will be attached to the chamber by tag welding without loss of the mechanical stability of the chamber material. The highest surface temperature is obtained at 5 GeV operation, when the center dipole is reversed in field direction and the field is increased to about twice the value for 18 GeV operation. In this case, the synchrotron radiation reaches the inside of the vacuum chamber inside the quadrupoles where the pump screen is located and where there is no cooling. The temperature reaches up to 210^{o}C at this point.

The gas load in the vacuum chamber is dominated by desorption of molecules from the chamber wall by synchrotron radiation photons (PSD). The photon flux at 10 GeV with a beam current of 2.7 A (worst case) is $8.1 * 10^{17} * \frac{E}{\mathrm{GeV}} * \frac{I}{\mathrm{mA}} = 2 * 10^{22}\mathrm{torr} * l * \mathrm{m}^{-1} * \mathrm{s}^{-1}$. A desorption coefficient in the order of η=$1 * 10^{-6} molecules/photon$ is assumed to be achieved after some conditioning. The desorbed gas load is then $1.3 * 10^{13} molecules/(\mathrm{sec} * \mathrm{m})$ or $4 * 10^{-7}\mathrm{torr} * \frac{l}{\mathrm{sec}*\mathrm{m}}$. The linear pumping speed is designed to be $100\, l/(\mathrm{sec} * \mathrm{m})$ which results in a pressure of 4 nTorr. This capacity is achieved by pumping slots which cover 10% of the surface of the pump screen corresponding to a conductance of $200\frac{l}{\mathrm{sec}*\mathrm{m}}$. Near the location of the quadrupole magnets, large lumped NEG cartridges and ion getter pumps are foreseen.

Due to the large beam currents, the RF-shielded bellows are a very critical element of the vacuum system design. The eRHIC design adapts the design which has been produced for the NSLS-II storage ring. The thermal contact of the sleeves is accomplished by fingers on the outside (see Figure 27). The NSLS-II design has shorter and wider fingers compared to the bellows designed for the Advanced Photon Source which minimizes the gaps in-between fingers and therefore avoids heating of the fingers by RF power leaking through the gaps.

Another critical element of the vacuum design is the RF seal of flange connections. The pre-conceptual design choice is to use soft RF springs. These require careful assembly and alignment to avoid steps and discontinuities in the vacuum chamber which would lead to considerable impedance and beam heating.

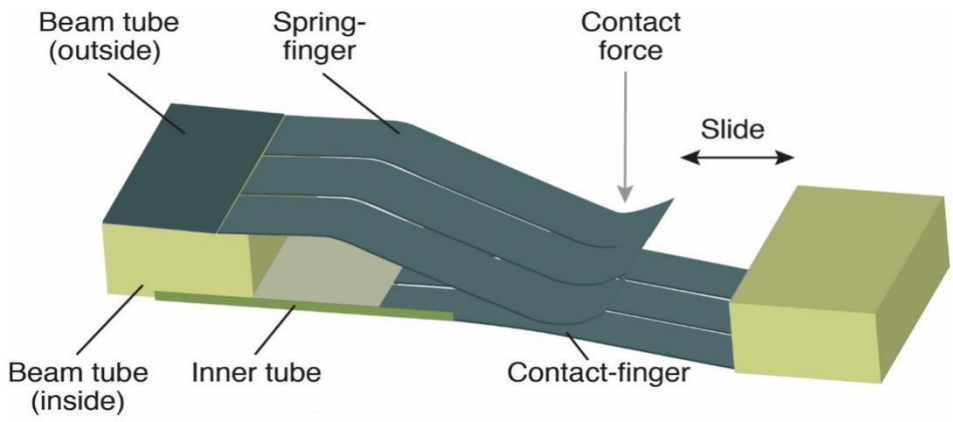

Figure 27: Schematic view of the bellow-finger concept

2.2.11.7 *RF System of Electron Storage Ring-Overview*

One limitation of the luminosity of the eRHIC electron-ion collider is the synchrotron radiation loss in the electron storage ring. The RF power needed to replace the synchrotron radiation losses of the high current electron beam with beam currents of up to 2.7 *A* and a beam energy of 10 GeV is 10 MW and requires an RF voltage of about 72 MV. The RF system is also the most costly hardware sub-system of the electron complex of eRHIC and its components need to be carefully optimized from both performance and cost point of view in the earliest stage of the design. Table 13 summarizes some relevant input parameters which determine the RF System.

Table 13: Summary of the eRHIC RF system requirements for 10GeV and 18GeV operations.

Parameter	*10GeV*	*18GeV*
Beam current [A]	2.7	0.27
Energy loss per turn [MeV]	3.7	37
Synchrotron radiation power [MW]	10	10
Required RF voltage [MV]	41	63

The choice of the electron cavities is based on superconducting RF resonators. The reasons for choosing superconducting RF cavities are as follow:

- Operational cost saving. For 18 GeV operation, the total power which would be required to generate the voltage of 63 MV in a normal-conducting cavity with typically $10\ \mathrm{M\Omega/m}$ shunt impedance and a maximum voltage of 2 MV/m would be approximately 12 MW. This is a large additional RF power which would have to be installed and operated. The additional power is much larger than the cryogenic power of 240 kW required to keep the cavities at 4 K. The additional RF installation would cost significantly more than the difference in cost for normal- and superconducting cavities.
- Superconducting cavities have a much higher (factor 9) stored field energy and are much better suited to handle heavy beam loading conditions.
- The impedances which drive coupled bunch instabilities are much lower than they would be for a normal-conducting cavity system with the same RF voltage.
- Because of the high gradient of superconducting cavities (8 MV/m vs. 2 MV/m for normal-conducting cavities), the superconducting cavities require less longitudinal space than normal conducting cavities.
- The disadvantage of superconducting cavities is their dependence on liquid He cooling and a more intricate protection system.

Superconducting RF systems are used in most light sources, as well as in KEKB and SuperKEKB. Technical solutions for such cavity systems based on single-cell 500 MHz resonators exist. The designs are mature and the systems are in principle commercially available. The available systems are, however, not optimized for high energy beam applications such as eRHIC. While the systems would work technically, the solution would not be optimum from a cost point of view. The eRHIC storage ring RF system is based on a dedicated and optimized concept of superconducting cavities:

- 2-cell 563 MHz cavities are designed for a more compact and cost effective RF structure.
- We developed a variable coupling, high power input coupler to run the system in various scenarios with optimized parameters for each beam energy and beam current.
- Novel RF power stations based on multiple IOT RF tubes lead to a cost effective design and require a relatively small footprint.

These design concepts lead to the parameters referenced in Table 14.

Table 14: Parameters of the eRHIC RF system.

Parameter	*Value*
RF frequency [MHz]	563
Number of cavity-cells per cryostat	2
Number of cryostats	16
Accelerating gradient [MV/m]	8
Maximum RF voltage [MV]	63
Maximum power per input coupler [kW]	500
Number of input couplers per cryomodule	2
Maximum RF output power [MW]	14
Number of RF transmitter stations	32
HOM power per cryomodule [kW]	28
HOM coupler type	Beam-pipe SiC
Beam pipe absorbers per cryostat	4

2.2.11.8 *Superconducting RF Cavities*

One 2-cell 563 MHz cavity is installed in each cryostat. The cavity shape has been optimized to suppress parasitic modes to the extent that the coupled bunch instabilities which are associated with the residual higher order modes (HOMs) can be safely controlled by a multi-bunch damper system. The broad-band impedance of the cavity structure is sufficiently low so there is no issue with single bunch instabilities. The cavity shape is depicted in Figure 28 and the higher order mode structure is shown in Figure 29.

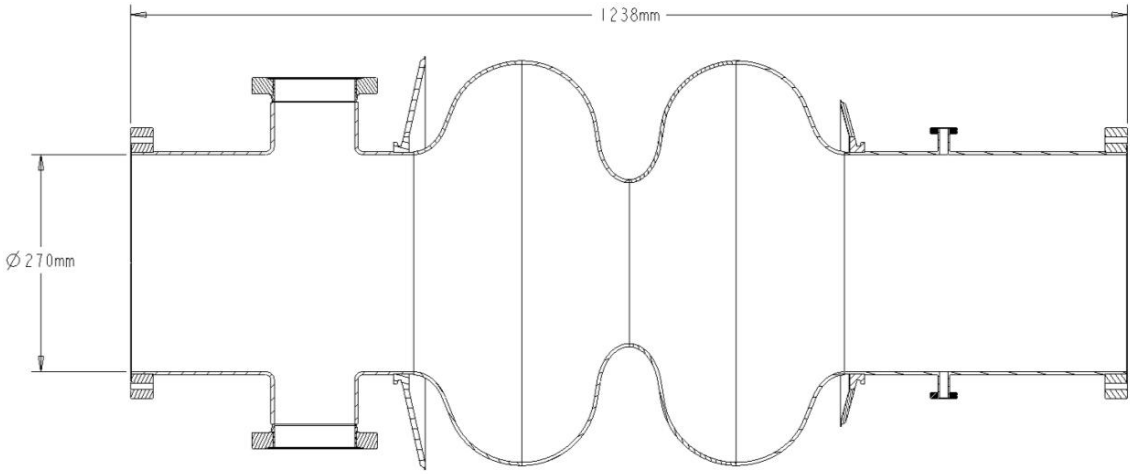

Figure 28: Optimized shape of the 2-cell 563 MHz superconducting cavity for eRHIC

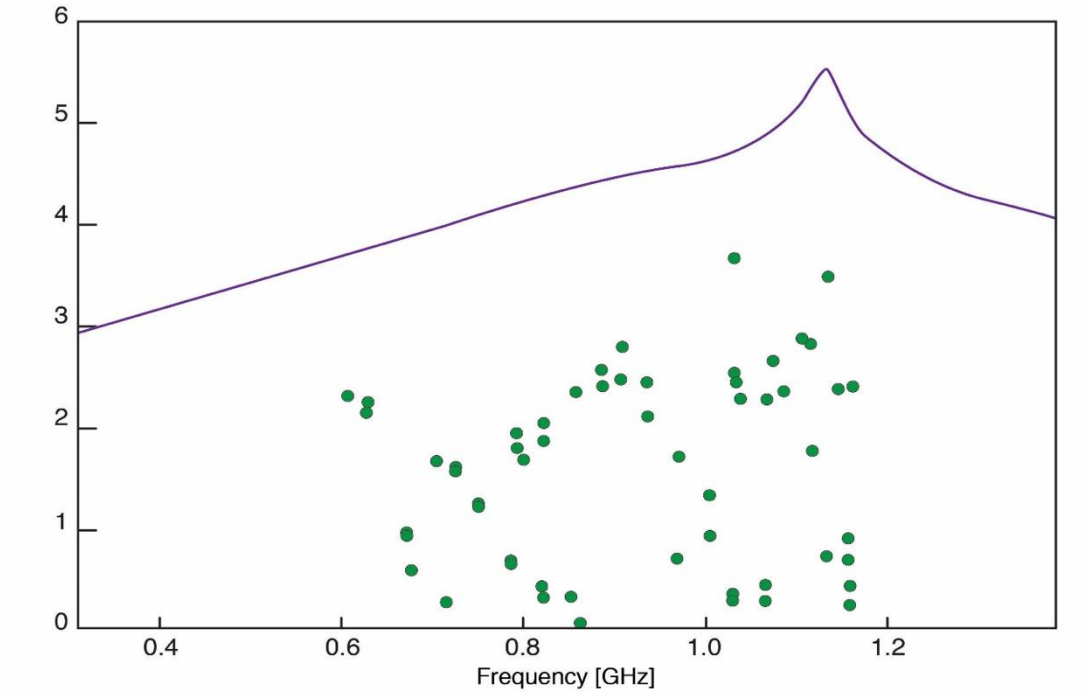

Figure 29: Longitudinal impedance of a single 2-cell cavity. The solid line is a Lorentzian fit of the envelope function; the dots are calculated using the code URMEL [25]. The vertical axis is impedance in units of kΩ .

Strong damping of higher order parasitic modes is important to achieve robust beam stability and to limit the required power of the broad-band damper system which actively stabilizes the beam. The choice made in the design of the eRHIC RF design is

to use beam-pipe type HOM dampers consisting of three well-cooled SiC sections of beam pipe
adjacent to each cavity. The SuperKEKB design [26] is adapted. Figure 30 depicts the RHIC SiC damper. Figure 31 shows a rendering of the new RF cavity design.

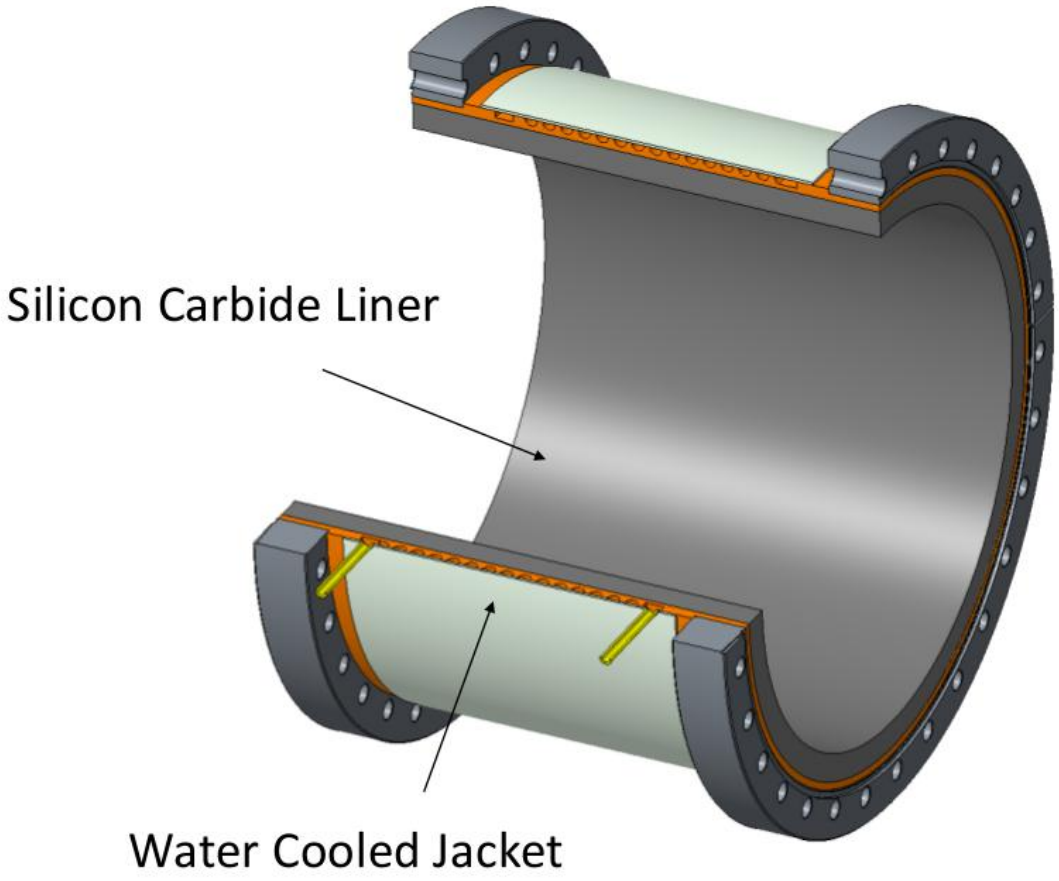

Figure 30: CAD model of the eRHIC SiC HOM damper (KEKB design)

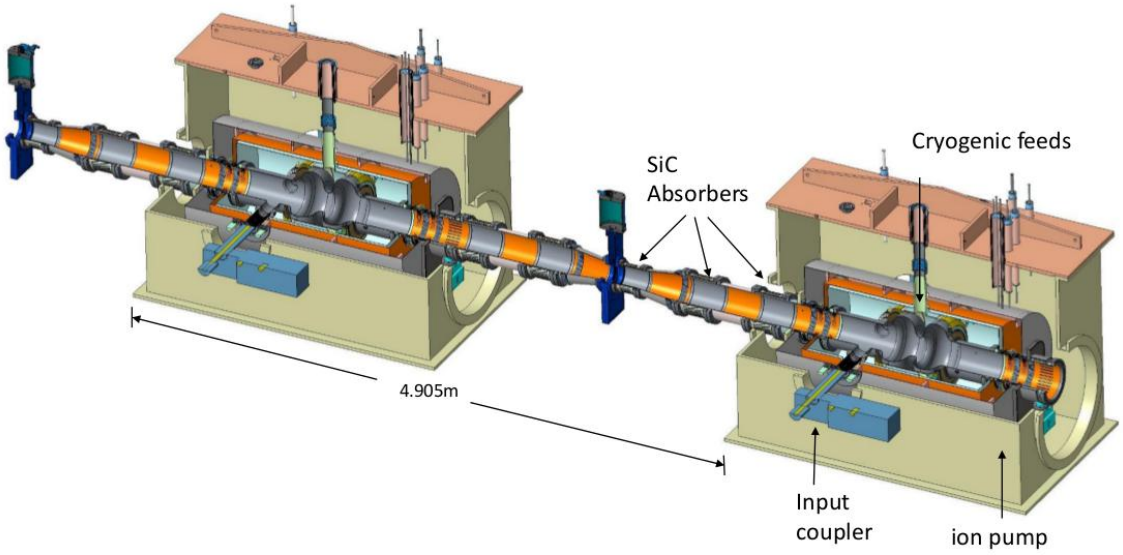

Figure 31: Rendering of the eRHIC two-cell superconducting cavity in a string of cryostats. Shown are two cryostats, each with a length of 4.0 m including the adjacent drift spaces with three SiC beam pipe absorbers, a taper and gate valves. Also shown are the cryogenic feeds and the RF input coupler. The cavity is enclosed in its liquid He tank

2.2.11.9 *High Power RF Input Complex*

The power capability of the fundamental power input coupler (FPC) is an important parameter for the layout of the RF system, since it determines the minimum number of cryomodules needed to feed 10 MW RF power to the beam. The choice was made to employ two 500 kW power couplers in each cryostat. Such a coupler had been designed and successfully tested with 500 kW for the superconducting photon gun developed at BNL. The eRHIC fundamental power coupler with two 500 kW arms is a development of this high power FPC.

The operation at different electron beam current and beam energies requires an optimized coupling of the superconducting cavities to their power source in order to avoid a large amount of reflected RF power. The optimum coupling is a function of the beam current, the synchronous phase, the shunt impedance, the power loss of the beam, and the cavity voltage. Figure 32 shows a CAD model of the eRHIC variable coupling high power input coupler.

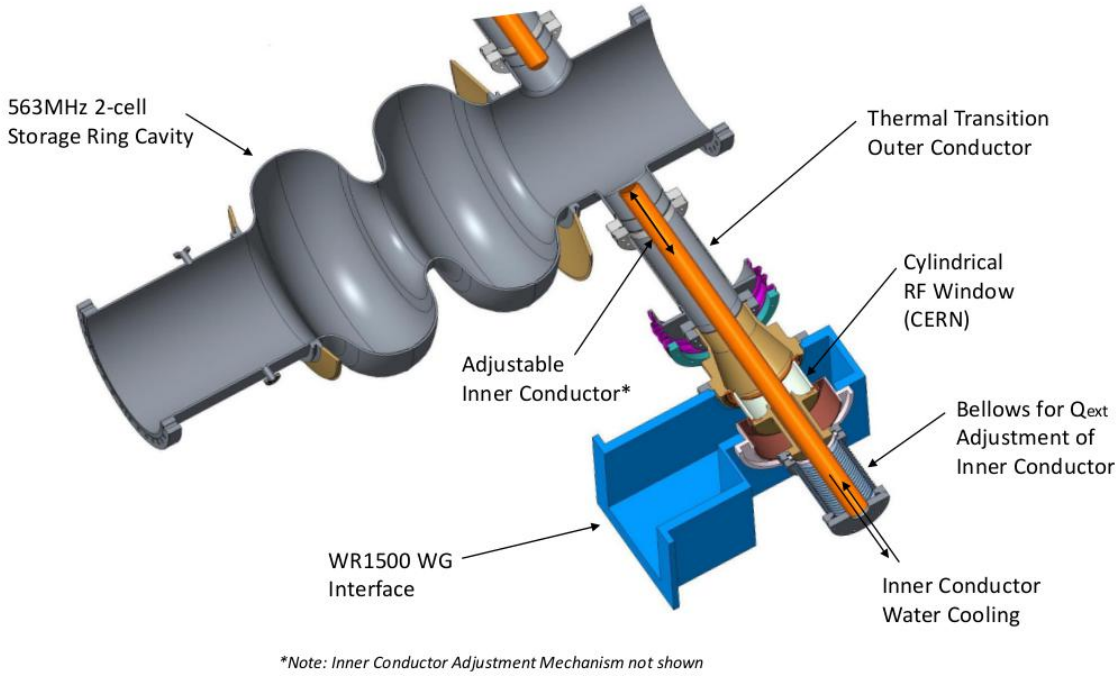

Figure 32: CAD model of the eRHIC 1 MW variable coupling double forward power coupler. Note that only one of the two 500 kW couplers is shown

2.2.11.10 *Electron Storage Ring RF Power Supply*

The RF power source of the eRHIC electron storage ring which has to deliver 10 MW of power to the beam is based on multi-IOT transmitters that can each generate 1 MW of RF power. The very large beam currents of the eRHIC electron storage ring with ion-clearing gaps in the bunch train cause substantial transient beam loading effects. The RF system has to provide a power margin of 15% to be able to control the RF voltage. The eRHIC collider will be operated with multi-purpose FPGA based cavity controller electronics which are designed to handle the large beam loading.

2.2.11.11 *Crab Cavities*

The eRHIC crab cavities, designed to operate at a frequency of 338 MHz, will be realized as superconducting Double Quarter Wave Crab Cavities (DQWCC). This cavity type, designed and developed at BNL for the LHC luminosity upgrade, has gone through a rigorous development program. The frequency of the LHC DQWCC devices is 400 MHz, conveniently close to the eRHIC DQWCC frequency, and thus serving to validate the expected performance of the eRHIC DQWCC.

At this time, a total of five LHC-style DQWCC have been built and tested with exceptionally good results: A proof-of-principle cavity built by Niowave Inc. for the BNL team and tested at BNL, two prototype cavities, designed by BNL, built by Niowave through a LARP program and tested at Jefferson Laboratory, and two prototype cavities of the same design built and tested at CERN. The BNL crab cavity team has been an active contributor to all the tests at JLab and CERN.

While the superconducting crab cavity is the most critical element of the crabbing system, there are many other auxiliary subsystems which are challenging and critical for

the proper crabbing of the beam. These subsystems, which will be described in detail in this document, include the liquid helium tank, HOM dampers, fundamental power and pickup couplers, mechanical cavity frequency tuner (comprising the dressed cavity, seen in Figure 33), as well as the crab cavity cryomodule. At this point all the subsystems mentioned have been built and successfully tested for the LHC DQWCC, and designed for the eRHIC DQWCC, using lessons learned from the LHC devices.

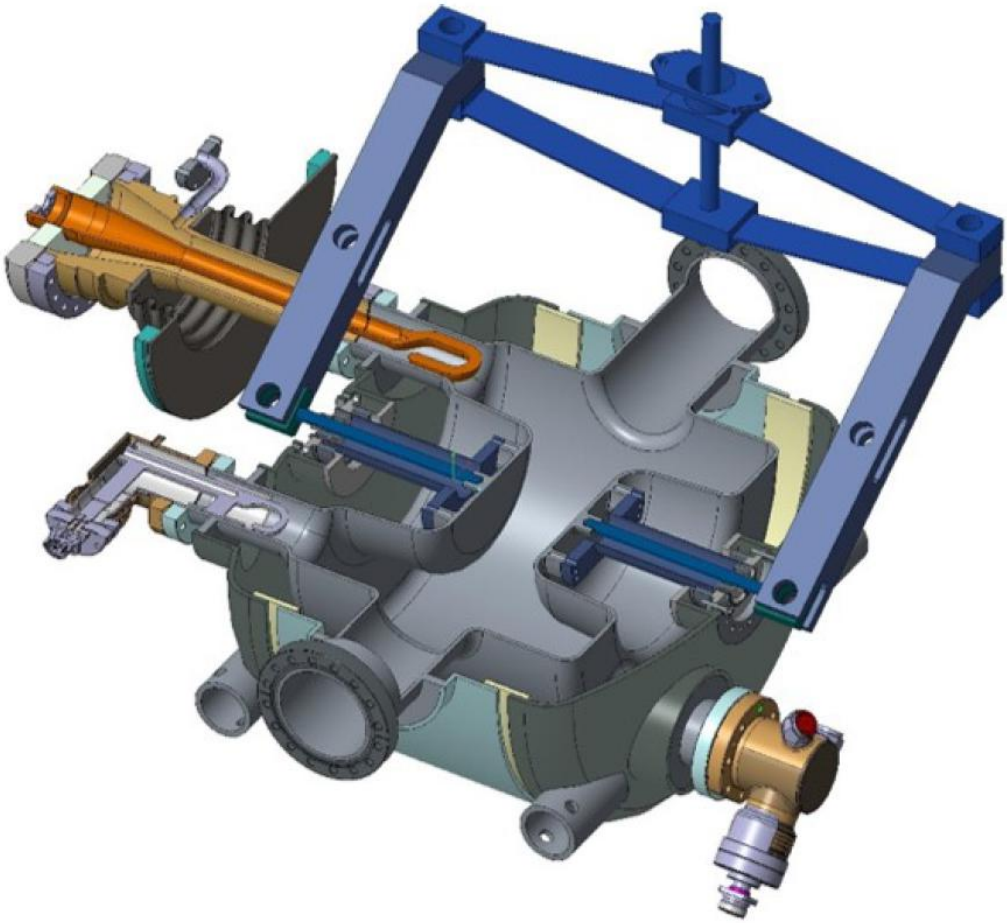

Figure 33: Cross section view of the eRHIC DQWCC showing the dressed cavity, with helium tank, couplers and tuner

The ultimate test of any accelerator cavity is its performance in the presence of beam. This is particularly true for hadron crab cavities, since there has never been any implementation of crab cavities in hadron accelerators. For this reason, a complete system, including two fully dressed DQWCC with all the couplers and tuners in a cryomodule, has been installed at CERN in the SPS accelerator, as can be seen in Figure 34 Beam tests are underway, with active participation of BNL staff.

Figure 34: The LHC prototype twin DQWCC cryomodule installed in the SPS tunnel for beam tests.

2.2.12 **Civil Construction and Infrastructure**

A major advantage of the eRHIC proposal is that only a modest amount of new buildings is required. At the present stage of the design, it is necessary to provide an industrial building at IR10 to house RF power sources for the electron storage ring and the rapid cycling synchrotron. A new building is also required for a 50 MeV superconducting LINAC which drives the electron cooling beam. The cryogenic capacity of the RHIC refrigerator is sufficient. However, at this point, the operation of the storage ring with 2 K liquid He is not excluded, which would allow a proton energy increase to 300 GeV. This choice would imply the necessity of a cold-compressor system in IR10 and IR4, respectively. The operation of RHIC does not require a large water cooling capacity whereas eRHIC operation requires cooling for the storage ring vacuum chamber with a capacity of 10 MW and for cooling room temperature magnets with a capacity of 7 MW.

The HVAC system in the RHIC tunnel requires a major upgrade in order to achieve thermal stability of stands and girders of the eRHIC magnet system.

2.2.13 **Summary**

The eRHIC collider as described provides collisions of electron and hadron beams stored in two storage rings, the Yellow ring of the Relativistic Heavy Ion Collider (RHIC) and a new electron storage ring, with high luminosity of $0 = 10^{34}\mathrm{cm}^{-2}\mathrm{sec}^{-1}$ over a center-of-mass energy range from 29 GeV to 140 GeV. The technical solution is based on accelerator physics and technology that is a moderate extrapolation of the state of the art. The required modifications of RHIC are few and relatively inexpensive on the scale of the entire project.

The challenge of the design lies in its implementation into an existing tunnel with existing infrastructure at a reasonable cost, which will require very detailed planning. The final factor of two to three in luminosity requires strong hadron cooling which will be realized by a novel scheme or by substantial extrapolation of existing technology. The main mitigation of the corresponding technical risk lies in the fact that a very respectable luminosity of up to $4.4 * 10^{33}\mathrm{cm}^{-2}\mathrm{sec}^{-1}$ can be achieved without strong hadron cooling, a performance which would provide full access to the entire EIC physics program.

The electron injector complex consists of a polarized electron gun and 400 MeV S-band LINAC which will provide polarized electron bunches of 10 nC to the rapid cycling synchrotron in the RHIC tunnel. This large synchrotron is to be constructed with normal-conducting magnets and normal-conducting RF systems. The critical requirement is high spin transparency for the polarized beam. This has been taken into account by special design features and has been tested by extensive simulations.

The anticipated performance of the collider has been addressed by a comprehensive accelerator physics design study. The design facilitates two large-solid-angle detectors utilizing the existing experimental areas now occupied by the RHIC detectors STAR and PHENIX/sPHENIX. Final parameters are chosen such that there is still a margin between the design values and values believed achievable. In that sense, the presented solution should be considered as robust and realistically achievable. While there are no components which require completely new technical concepts, several components are at state-of-the-art or slightly beyond present technology. The list of these components includes special superconducting magnets in the interaction regions with very large apertures and with active magnetic shielding. Other advanced components are 2-cell superconducting cavities with 1 MW of input power and variable coupling of the forward power couplers. Strong hadron cooling requires a CW electron source which can deliver reliably 100 mA of beam current.

2.2.14 **References**

1. D. Kayran et al., Proof-of-Principle Experiment for FEL-based Coherent Electron Cooling, Conf. Proc., C110328:2064-2066
2. A. A. Sokolov and I. M Ternov, Polarization and spin effects in the theory of synchrotron radiation, Doklady Akademii Nauk SSSr (USSR), English translation currently published in a number of subject-oriented journals, 153, 1963
3. E. C. Aschenauer et al., eRHIC Design Study: an Electron-Ion Collider at BNL, 2014. arXiv:1409.1633
4. A. Accardi et al., Electron Ion Collider: The Next QCD Frontier, Eur. Phys. J., A52(9):268, 2016. arXiv:1212.1701, doi:10.1140/epja/i2016-16268-9
5. N. Toge, KEK B-Factory Design Report, Technical report, 1995
6. PEP-II: An Asymmetric B-Factory. Conceptual Design Report. June 1993
7. V. N. Litvinenko and Y. S. Derbenev, Coherent Electron Cooling. Phys. Rev. Lett. 102:114801, 2009. Doi:10.1103/PhysRevlett.102.114801
8. K. Ohmi, Simulation of beam-beam effects in a circular e^+e^- collider. Phys. Rev. E62:7287-7294, 2000. Doi:10.1103/PhysRevE.62.7287
9. J. Qiang, M. A. Furman, and R. D. Ryne, A parallel particle-in-cell model for

beam-beam interacton in high energy ring colliders. J. Comput. Phys., 198:278-294, 2004. doi:10.1016/j.jcp.2004.01.008
10. B. Parker et al., Compact superconducting final focus magnet options for the ILC. Conf. Proc., C0505161:1569, 2005
11. V. Ptitsin and Yu. M. Shatunov, Helical spin rotators and snakes. Nucl. Instrum. Meth., A398:126-130, 1997. doi:10.1016/S0168-9002(97)00683-9
12. I. Alekseev et al., Polarized proton collider at RHIC. Nucl. Instrum. Meth., A499:392-414, 2003. doi:10.1016/So168-9002(02)01946-0
13. D. P. Barber et al., The first achievement of longitudinal spin polarization in a high-energy electron storage ring. Phys. Lett., B343:436-443, 1995. doi:10.1016/0370-2693(94)01465-0
14. Yuri Shatunov and Vadim Ptitsin, Siberian Snkes for electron Storage Rings. Conf. Proc., C970512:3500, 1997
15. I. Borchardt, E. Karantzoulis, H. Mais, and G. Ripken, Calculation of Beam Envelopes in Storage rings and Transport Systems in the Presence of Transverse Space Charge Effects and Coupling, Z. Phys., C39:339, 1988
16. D. P. Barber et al., Longitudinal Positron Polarisation in HERA-II. In 9th European Particle Accelerator Conference (EPAC2004), Lucerne, Switzerland, July 5-9, 2004. URL: http://accelconf.web.cern.ch/AccelConf/e04/PAPERS/MOPLT044.PDF
17. Y. S. Derbenev and A. M. Kondratenko, Diffusion of particle spins in storage elements. Sov. Phys. JETP,35:230, 1972
18. R. Assmann et al., Deterministic harmonic spin matching in LEP. Conf. Proc., C940627:932-934, 1994
19. J. Laskar et al., The measure of chaos by the numerical analysis of the fundamental frequencies. Application to the standard mapping. Physica, D56:253-269, 1992. doi:10.1016/0167-2789(92)90028-L
20. M. Blaskiewicz, A multipurpose coherent instability simulation code. In: particle Accelerator Conference (PAC 2007), p. 3690-3692, 2007
21. O. S. Bruning et al., Electron cloud and beam scrubbing in the LHC. In Proc. 1999 Particle Accelerator Conference (PAC'99), New York, New York, March 29-April 2, 1999. P. 2629-2631, 1999. URL: http://accelconf.web.cern.ch/AccelConf/p99/PAPERS/THA6.PDF
22. M. Blaskiewicz and U. Iriso, How to use CSEC. Technical report, Brookhaven National Laboratory (BNL) Relativistic Heavy Ion Collider, 2006
23. A. Piwinski, Intra-beam Scattering. In proc. 9th International Conference on High-Energy Accelerators (HEACC 1974), Stanford, CA, May 2-7, 1974, p. 405-409, 1974
24. D. Ratner, Microbunched Electron Cooling for High Energy Hadron Beams. Phys. Rev. Lett., 111(8):084802, 2013. doi:10.1103/PhysRevLett.111.084802
www.cst.com
25. T. Tajima et al., Development of HOM damper for B-Factory (KEKB) superconducting cavities. Conf. Proc., C950501:1620-1622, 1996
26. V.N. Baier, V.M. Katkov, V.M. Strakhovenko, Sov. Phys. JETP. 31 (1970) 908
27. J. Kewisch, Computation Of Electron Spin Polarization In Storag Rings, Proceedings, Europhysics Conference, Berlin, Germany, September 20-23, 1983, 249-254, 1985.

28. L. H. Thomas, "The Kinematics of an electron with an axis," Phil. Mag. 3, 1–21 (1927).
29. V. Bargmann, L. Michel, and V. L. Telegdi, Phys. Rev. Lett. 2, 435–436 (1959).
30. D.P. Barber et al., High spin polarization at the HERA Electron Storage Ring, Nucl. Instrum. Methods A **338**, 166-184 (1994).

2.3 JLEIC – A Polarized Electron-Ion Collider at Jefferson Lab

JLEIC Design Study Collaboration
(Edited by Todd Satogata and Yuhong Zhang)
Thomas Jefferson National Accelerator Facility, Newport News, Virginia, USA
Mail to: satogata@jlab.org and yzhang@jlab.org (editors)

2.3.1 Introduction

Todd Satogata and Yuhong Zhang
Thomas Jefferson National Accelerator Facility, Newport News, Virginia, USA
Mail to: satogata@jlab.org and yzhang@jlab.org

Modern nuclear physics has led to the development of Quantum Chromo-Dynamics (QCD), a theory describing strong interactions among quarks and leptons, and gluons as the carriers of the strong force. Understanding these interactions as well as the emergent properties of nucleons and nuclei from these interactions is the compelling goal of nuclear science. A polarized electron-ion collider (EIC) has long been envisioned as a gluon microscopy for exploring the QCD frontier. To meet this science need, Jefferson Lab has proposed JLEIC, a high luminosity high polarization EIC based on the CEBAF electron SRF linac. The JLEIC design was driven by the science program summarized in an EIC white paper [1], and significant design studies and accelerator R&D has been pursued and achieved over the last 16 years. In the following, a set of articles are collected to describe the JLEIC design and to report progress of the related accelerator R&D. The topics covered by these articles are ion sources, polarized electron source, polarization of electron and proton/light ion beams, electron cooling and high energy ERL cooler, beam-beam and other collective beam physics, ion ring magnets, interaction region design and special magnets.

During the last 6 years, two comprehensive reports [2,3] were produced on 2012 and 2015 respectively for summarizing the JLEIC design and accelerator R&D progress. It should also be mentioned that the JLEIC electron-ion collider design study was also reported and reviewed in the two early issues (April, 2003 and August, 2012) of the ICFA Beam Dynamics Newsletter. Presently, the JLEIC collaboration is writing a pre-Conceptual design report (CDR) [4] which is targeted for a public release at the end of October, 2018.

We would like to take this opportunity to acknowledge the valuable contributions by members of Jefferson Lab JLEIC accelerator design team and many external collaborators. These collaborators are from many US and international institutions which are listed below: Argonne National Laboratory, Brookhaven National Laboratory, Fermi National Laboratory, Lawrence Berkeley National Laboratory, SLAC National